https://doi.org/10.5194/os-2022-19
Preprint. Discussion started: 1 April 2022

Ocean Science
Discussions
Open Access
EGU

The role of tides and sea ice on the carbonate chemistry in a coastal polynya in the south-eastern Weddell Sea

Elise Droste[1], Mario Hoppema[2], Melchor González-Dávila[3], Juana Magdalena Santana-Casiano[3], Bastien Y. Queste[1,4], Giorgio Dall'Olmo[5], Hugh J. Venables[6], Gerd Rohardt[2], Sharyn Ossebaar[7], Daniel Schuller[8], Sunke Trace-Kleeberg[2,9], and Dorothee C. E. Bakker[1]

[1]School of Environmental Sciences, University of East Anglia, Norwich Research Park, NR4 7TJ Norwich, United Kingdom
[2]Alfred Wegener Institute Helmholtz Centre for Polar and Marine Research, Postfach 120161, 27515 Bremerhaven, Germany
[3]Instituto de Oceanografía y Cambio Global, IOCAG, Universidad de Las Palmas de Gran Canaria, ULPGC, 35017 Las Palmas de Gran Canaria, Spain
[4]Department of Marine Sciences, University of Gothenburg, Carl Skottsbergs Gata 22B, SE-413 19 Gothenburg, Sweden
[5]Plymouth Marine Laboratory, Prospect Place, PL1 3DH Plymouth, United Kingdom
[6]British Antarctic Survey, High Cross, Madingley Road, CB3 0ET Cambridge, United Kingdom
[7]NIOZ Royal Netherlands Institute for Sea Research, department of Ocean Systems, P.O. Box 59, 1790 AB, Den Burg, Texel, The Netherlands
[8]Scripps Institution of Oceanography, UC San Diego, 8622 Kennel Way, La Jolla, CA 92037, United States
[9]School of Ocean and Earth Science, National Oceanography Centre, University of Southampton, Southampton, SO14 3ZH, United Kingdom

Correspondence: Elise Droste (e.droste@uea.ac.uk)

Abstract.

Tides significantly affect polar coastlines by modulating ice shelf melt and modifying shelf water properties through transport and mixing. However, the effect of tides on the marine carbonate chemistry in such regions, especially around Antarctica, remains largely unexplored. We address this topic with two case studies in a coastal polynya in the south-eastern Weddell Sea, neighbouring the Ekström Ice Shelf. The case studies were conducted in January 2015 (PS89) and January 2019 (PS117), capturing semi-diurnal oscillations in the water column. These are pronounced in both physical and biogeochemical variables for PS89. During rising tide, advection of sea ice melt water from the north-east created a fresher, warmer, more deeply mixed water column with lower dissolved inorganic carbon (DIC) and total alkalinity (TA) content. During ebbing tide, water from underneath the ice shelf decreased the polynya's temperature, increased the DIC and TA content, and created a more stratified water column. The variability during the PS117 case study was much smaller, as it had less sea ice melt water input during rising tide and was better mixed with sub-ice shelf water. The contrasts in the variability between the two case studies could be wind and sea ice driven, and underline the complexity and highly dynamic nature of the system.

The variability in the polynya induced by the tides results in an air-sea CO_2 flux that can range between a strong sink (-20 mmol m^{-2} day^{-1}) and a small source (7 mmol m^{-2} day^{-1}) on a semi-diurnal time scale. If the variability induced by tides is not taken into account, there is a potential risk of overestimating the polynya's CO_2 uptake by 98 % or underestimating it by 108 % (mistaking it for a source instead of a variable sink), compared to the average flux determined over several days. Given the disproportionate influence of polynyas on heat and carbon exchange in polar oceans, we recommend that future studies

https://doi.org/10.5194/os-2022-19
Preprint. Discussion started: 1 April 2022

around the Antarctic and Arctic coastlines consider the timing of tidal currents in their sampling strategies and analyses. This will help constrain variability in oceanographic measurements and avoid potential biases in our understanding of these highly complex systems.

1 Introduction

Coastal regions are subject to tidal forces, which modify the water column through enhanced mixing (Padman et al., 2009). Tides in polar regions have recently gained increasing attention in investigations focusing on understanding the physical interaction between the ocean and sea ice (e.g., Dmitrenko et al., 2012; Kirillov et al., 2013; Skogseth et al., 2013) and how they affect ice shelf melt (e.g., Makinson et al., 2011; Mueller et al., 2018; Padman et al., 2018; Huot et al., 2021). Tidal effects on the biogeochemistry along polar coastlines, however, have not yet received similar attention, even though tides have been shown to affect the chemical properties and the fugacity of seawater CO_2 (fCO_2) in other regions (Rogachev et al., 2001; Andersson and MacKenzie, 2012; Sims et al., 2022).

Areas of open water in the middle of an otherwise sea ice covered region, also known as polynyas, are common features along polar coastlines. They are well known for their contribution to sea ice formation (Renfrew, 2002) and both heat and carbon exchange with the atmosphere (Hoppema and Anderson, 2007). They have been described as “windows" between the ocean and the atmosphere (Barber and Massom, 2007), enabling strong interaction between these two spheres in regions and at times of the year when sea ice cover would otherwise restrict it. They are therefore thought to have a disproportionally large impact on the polar oceans considering their relatively small surface area (Barber and Massom, 2007). The prolonged ice-free conditions allow direct gas exchange to occur, a longer time window for equilibration of CO_2 with the atmosphere, as well as prolonged biological productivity (Hoppema and Anderson, 2007). Substantial biological activity is observed in coastal polynyas around the Antarctic continent (Arrigo and van Dijken, 2003). This makes them important with regard to air-sea CO_2 flux estimates.

In shallow and coastal regions, tides can have an important role in modulating the physical and biogeochemical properties of the polynya’s water column, especially along its margins. In particular, the effect of tides on the marine carbonate chemistry remains largely unexplored. Understanding the tidal influence may help us to quantify some of the variability observed in biological productivity around Antarctica (Arrigo et al., 2015) and the capacity of coastal polynyas to absorb CO_2. Practically, understanding the role of tides can help develop more reliable sampling activities that consider the timing and strength of tidal currents, thereby obtaining representative data of a highly dynamic system.

The tides in the Weddell Sea are the largest in the Southern Ocean (Padman et al., 2018). Here, relatively warm, carbon-rich Warm Deep Water (WDW) upwells in the east and is physically and chemically altered along its route towards the western Weddell Sea, a hotspot for Antarctic Bottom Water (AABW) formation and natural carbon sequestration (Fahrbach et al., 1994;

https://doi.org/10.5194/os-2022-19
Preprint. Discussion started: 1 April 2022

Anderson et al., 1991; Huhn et al., 2013). Water on the eastern shelf is modified through ventilation with the atmosphere and also has the potential to be exported to the deep ocean by northward transport into the Upper Circumpolar Deep Water (uCDW) (Orsi et al., 2002), along with any CO_2 that has been exchanged with the atmosphere at the continental shelf. Studying processes that modify the physical and chemical properties of these deep water masses, such as tides, will enable a better understanding of the transport of anthropogenic carbon to the deep ocean.

In this work, we illustrate the effect of tides on the seawater carbonate chemistry with two case studies in a coastal polynya in the south-eastern Weddell Sea that neighbours the Ekström Ice Shelf (Fig. 1). This coastal polynya regularly forms in the summer months (Boebel, 2019; Arrigo and van Dijken, 2003; Arrigo et al., 2015). Coastal polynyas in this region are typically formed by katabatic winds from the continent that advect the newly produced sea ice away from the coastline in the spring and summer (Eicken and Lange, 1989; Renfrew, 2002). At the Ekström Ice Shelf, a number of grounded ice bergs to the east can also create a sea-ice free lee downstream from the westward-flowing coastal current (Boebel, 2019). We will present biogeochemical observations for two separate and independent tidal sampling campaigns in the austral summer: one in January 2015 and the other in January 2019. To the best of our knowledge, this is the first time that tidal influences on the seawater carbonate chemistry are studied in a coastal Antarctic polynya. We discuss the variability induced by tidal forces and explore the differences between the two tidal observations in terms of their physical and biogeochemical characteristics, and what it means for ocean CO_2 uptake.

2 Methods

2.1 Sample collection and measurements

The data were collected during two repeat hydrographic expeditions in the Weddell Sea with the German icebreaker *R.V. Polarstern*: expedition PS89 (2 December 2014 - 31 January 2015; Cape Town - Cape Town; (Boebel, 2015)) and expedition PS117 (12 December 2018 - 7 February 2019; Cape Town - Punta Arenas; (Boebel, 2019)). During both expeditions, the tidal cycle was recorded by means of repeat CTD casts at the same location at a frequency that was high enough to constrain the tidal oscillation in the water column. These recordings will hereafter be referred to as *tidal observations*. The tidal observations were performed at the same site in a coastal polynya, 56 km west of Atka Seaport, directly at the edge of the Ekström Ice Shelf (Fig. 1), the geometry of which is thought to be representative of most ice shelves of Dronning Maud Land (Smith et al., 2020a).

Coastal polynyas in the eastern Weddell Sea have an average area of 7.75 x 10^3 km^2 in the summer and 1.12 x 10^3 km^2 in winter (coastal polynyas numbers 12-17 in Arrigo and van Dijken (2003)). The size and shape of the polynyas at the Ekström Ice Shelf are highly variable, depending on the wind direction and speed. For the PS89 tidal observations, the average width (between the ice shelf and sea ice) of the Ekström polynya is about 0.8 km, estimated from Synthetic Aperture Radar (SAR) images (Fig. A1). The length was approximately 12 km. During the PS117 tidal observation, the polynya was substantially larger, having an approximate average width of 3 km and a length of about 40 km (Fig. A3). Generally, the polynya during both tidal observations at this location is considered to be relatively small.

https://doi.org/10.5194/os-2022-19
Preprint. Discussion started: 1 April 2022

Information about the tidal observations is shown in Table 1. Sources of supporting data used in this study can be found in the Supplementary Materials (Table B1). Both tidal observations were made at the same time of year (i.e. mid-January). The sampling during PS89 (75 hours) lasted ∼3 times longer than during PS117 (22 hours). The exact location of the hydrographic stations differed slightly between the two expeditions due to shifting of the Ekström Ice Shelf extent between 2015 and 2019. The sampling sites for PS117 were chosen in such a way that the distance to the ice shelf was approximately the same as during PS89. Due to other ongoing scientific activities on board during the PS117 tidal observation, the exact location of sampling within the coastal polynya varied slightly per CTD cast, but the casts remained within a maximum distance of 300 m from each other. The polynya is bordered by the Ekström Ice Shelf along its southern edge, and by sea ice along the rest of its perimeter.

In addition to a SBE911plus CTD sensor, each rosette sampler (SBE32, 24 x 12 L bottles) was equipped with a fluorometer (EcoFLR, Wetlabs), an oxygen optode (SBE43, Seabird Electronics), and an Acoustic Doppler Current Profiler (ADCP) system (2x 300 kHz RDI Workhorse ADCPs) (Table C1). The oxygen measurements were calibrated using discrete oxygen samples from deep CTD casts only, analysed with the Winkler method (Boebel, 2015, 2019; Rohardt and Tippenhauer, 2020). The oxygen optode sensor was malfunctioning on every other cast during the PS117 tidal observation period and thus its data had to be excluded from further analysis.

Dissolved inorganic carbon (DIC) and total alkalinity (TA) samples were collected following Dickson et al. (2007). DIC and TA samples were analysed on a VINDTA 3C system (Mintrop, 2016), which uses coulometry for DIC and potentiometric titration for TA determination. TA was calculated according to Dickson et al. (2007) for PS89 and using the Python package Calkulate (Humphreys and Matthews, 2022) for PS117. On PS89, dissolved phosphate (PO_4^{3-}), silicate (SiO_4), and nitrate (NO_3^-) analyses performed by UV-Vis spectrophotometric methods were carried out on board with a SEAL Analytical continuous-flow AutoAnalyzer (Boebel, 2015). During PS117, nutrient samples were analysed simultaneously for PO_4^{3-}, SiO_4, nitrite (NO_2^-), and the combination of $NO^{3-} + NO_2^-$ on board on a continuous gas-segmented flow TRAACS 800 Auto-Analyzer (Technicon, a.k.a. SEAL Analytical) within 4-5 hours after sampling (Boebel, 2019). Samples were calibrated with standards diluted in low nutrient sea water within the salinity range of the Southern Ocean. Analytical uncertainties can be found in Tables C2 and C3 .

To complement the ADCP data, a tidal model (Model CATS2008) was used to determine the times of high (rising) and low (ebbing) tide during the tidal experiments. This model has been optimised for the Antarctic seas, using available measurements and including ice shelf cavities to improve performance (Padman et al., 2002). All tidal constituents, which represent each mode of the tidal oscillation on a different time-scale, are used (e.g. M2, S2, K1). The modelled currents are averaged over the entire water column for tidal currents only, i.e. they are not total currents. Total currents (measured by the ADCP) include contributions from, for example, mean flow along the continental shelf.

https://doi.org/10.5194/os-2022-19
Preprint. Discussion started: 1 April 2022

Ocean Science
Discussions
Open Access
EGU

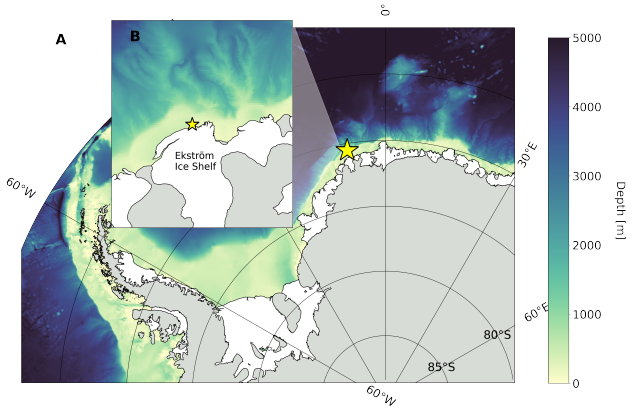

Figure 1. Map of study site: A) Weddell Sea with bathymetry. Grey regions represent the Antarctic continent and land-fast ice, white regions represent ice shelves. B) Enlarged map of coastal study site along the Ekström Ice Shelf. Yellow star shows location of tidal measurements. See Table 1 for coordinates.

Table 1. Details of the tidal observations made with repeat CTD casts and discrete seawater sampling during the two hydrographic expeditions: PS89 and PS117.

	PS89	PS117
Start observations [UTC]	21:09 9 Jan. 2015[a]	14:27 11 Jan. 2019
End observations [UTC]	01:00 11 Jan. 2015	11:57 12 Jan. 2019
Location	70° 31' 24" S	70°31' 19.56" S
	8° 45'34.2" W	8°46' 6.76" W
Deepest depth of CTD cast	160 m	190.5 - 201.5 m
No. of CTD casts	40	8
No. DIC/TA bottle samples	260	67

[a]Two casts done on the 8^{th} of January have not been included into this case study. ADCP measurements started on the 7th of January. The underway fCO_2 measurements started on the 7^{th} of January at 23:00.

2.2 CO_2 flux calculations

The air-sea CO_2 flux was calculated according to:

$$F = kK_0(fCO_{2sw} - fCO_{2atm}) \quad (1)$$

F is the CO_2 flux in mol m^{-2} hr^{-1}, k is the gas transfer velocity, K_0 is the CO_2 solubility at *in situ* temperature and salinity, and fCO_2 is the fugacity of CO_2 in seawater (sw) and in the atmosphere (atm). The gas transfer velocity is calculated according to the parameterisation of Wanninkhof (2014). Minimum, maximum, and average wind speed for the duration of the

https://doi.org/10.5194/os-2022-19
Preprint. Discussion started: 1 April 2022

tidal observation period, as measured on board and reported at 10 m above sea level, were used as input to this parameterisation. For the Schmidt number, i.e. the parameter that relates the gas transfer velocity of different gases, we use Wanninkhof (2014), which gives a refitted polynomial updated from Wanninkhof (1992) to cover a temperature range of -2 to 40 °C and is virtually the same as the parameterisation by Ho et al. (2006). The CO_2 solubility is calculated according to Weiss (1974). The fugacity of CO_2 is numerically similar to the partial pressure of CO_2 (pCO_2), but accounts for the non-ideal behaviour of the gas. The fCO_{2atm} is calculated using the virial- and cross-virial coefficients from Weiss (1974) in the equation to convert the atmospheric CO_2 mole fraction to fCO_2 by Weiss and Price (1980). It requires the dry air mole fraction of CO_2 (xCO_2), for which we use discrete air sample measurements from Syowa Station (Dlugokencky et al., 2019), and the water vapour pressure, which is derived from *in situ* seawater temperature and salinity in the parameterisation of Weiss and Price (1980). We use the average xCO_2 of January 2015 and 2019 for the PS89 and PS117 experiment, respectively, and shipboard atmospheric pressure reported at sea level.

The fCO_2 of surface seawater (fCO_{2sw}) is determined from the DIC and TA concentrations of the shallowest discrete seawater values (typically between 15 and 5 m deep), using PyCO2SYS (Version 1.3) (Humphreys et al., 2022), based on the original work of Lewis and Wallace (1998). Additionally, continuous surface water fCO_2 was measured at the ship's seawater supply with an intake at 11 m depth by a General Oceanics pCO_2 analyser on board, for the PS89 tidal observation only. The discrete surface seawater samples were collected at the same depth as the underway water intake depth (∼11 m) or shallower (∼5 m). The measured and calculated fCO_2 values are comparable for the periods where they overlap (Fig. D1). Small discrepancies between the measured and calculated values are likely due to the difference in depth and spatial and temporal variability.

3 Results

3.1 Tidal current

The *u* (east-west) and *v* (north-south) components of the current velocity measured by the ADCP are significantly positively correlated to each other (Fig. F1). They synchronously alternate sign roughly twice a day throughout the water column (Padman et al., 2002), resulting in a barotropic (depth-averaged) component of the flow that matches the modelled tidal velocity (Fig. 2). The semi-diurnal tidal currents are thus a dominant component of the total current velocity at this sampling location. The vertical grey areas in Fig. 2 (and in other figures) indicate the time and duration of ebbing tide, here defined as the time when both the *u* and *v* components of the current velocity are positive, i.e. the direction of the current is towards the north-east. When both components are negative, the direction is towards the south-west and here considered to be rising tide. Note that the white vertical areas in the figures include the rising tide as well as times when either the *u* or *v* component is negative.

The velocity profiles are generally homogeneous during ebbing tide. More vertical structure is seen in both velocity components after peak velocities are reached during rising tide during PS89. These baroclinic (depth-dependent) flows induce short-lived vertical shear between the surface and subsurface layers before velocity profiles homogenise again towards the north-east (ebb). The range of current velocities is slightly larger during the PS89 tidal observation than during PS117 (Fig.

https://doi.org/10.5194/os-2022-19
Preprint. Discussion started: 1 April 2022

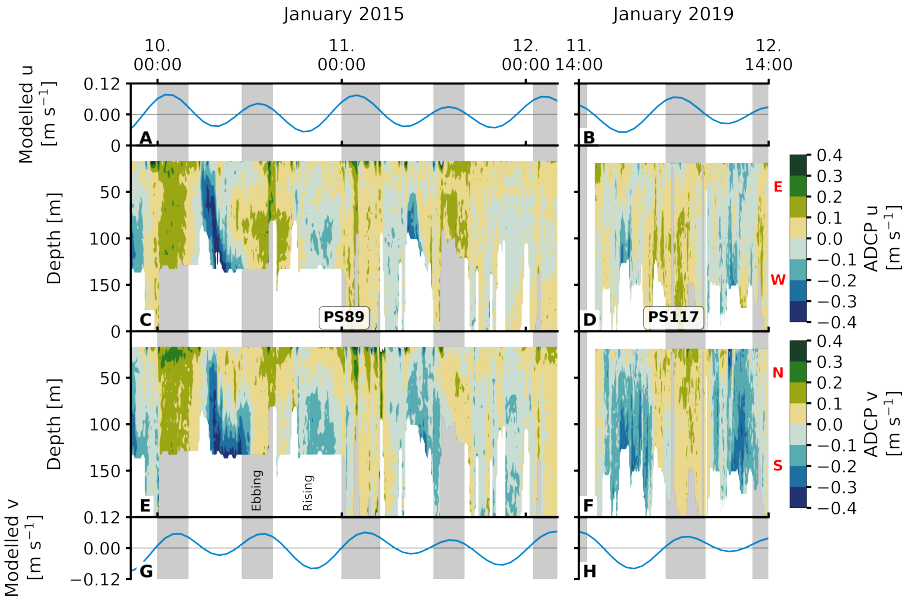

Figure 2. Current velocity for PS89 (A, C, E, G) and PS117 (B, D, F, H). Modelled *u* component of the tidal currents is shown in panels A and B. The modelled *v* component is shown in G and H. Modelled tidal velocities are averaged over the full water column. The*u* component of the ADCP profile data is shown in C and D. The *v* component of the ADCP data is shown in E and F. Vertical grey areas indicate times of ebbing tide, here identified as times when the *u* and *v* components in the modelled tidal current are both positive, i.e. the direction of the current is north-east. Directions associated to the positive and negative values of the *u* and *v* components are indicated by the red letters next to the colour bars: N (north), S (south), E (east), W (west).

F1), which is mainly due to the higher velocities in the morning of 10 January 2015. The modelled tidal current at this time is not particularly stronger than at any other time point in the observation period, including PS117. The stronger current in the first half of 10 January 2015 is thus likely the result of other enhancing factors, such as wind speed and direction.

Both the PS89 and PS117 discrete tidal observations were made five days after spring tide, although the spring tide prior to the PS89 observations was at full moon (5 January 2015) and the spring tide prior to the PS117 observations was at new moon (6 January 2019; dates obtained from https://tidesandcurrents.noaa.gov/historic_tide_tables.html). The tidal observations of both case studies are thus set at a similar time in the spring-neap tidal cycle. Peak-to-peak tidal heights in this region are around 2 m, but may increase by a factor of two during spring tides (Padman et al., 2002, 2018). Our datasets only capture a small fraction of time, and we cannot judge the relative strength of the tide beyond its time limits. However, considering that the dominant constituent of tidal oscillations in the Weddell Sea is the semi-diurnal constituent (Padman et al., 2002) and that the modelled velocities are similar between both tidal observations, we regard the two case studies as comparable in terms of tidal influence on the system.

https://doi.org/10.5194/os-2022-19
Preprint. Discussion started: 1 April 2022

3.2 Physical variability

A clear semi-diurnal tidal cycle is observed in the physical properties of the water column during the PS89 tidal observation period in January 2015 (Fig. 3). Over the depth horizons, salinity increases and temperature decreases throughout the water column during ebbing tide. Isopycnals rise to the surface, resulting in a shallow stratification. A mixed layer forms at the surface during ebbing tide with relatively uniform properties and an average depth of ∼20 m. The mixed layer depth (MLD) is determined by a 0.02 kg m^{-3} density difference with the average of the top 10 m. During rising tide, the MLD tends to either deepen or the mixed layer breaks down altogether as the density decreases. When a steep density gradient is absent, which typically occurred during rising tide, the water column is considered to be relatively well mixed. The isolines for salinity and temperature deepen as the surface water becomes fresher and warmer. These semi-diurnal fluctuations occur throughout the water column, down to the bottom at almost 200 m depth.

While a similar tidal pattern is also recorded in the salinity and temperature profiles of the shorter PS117 tidal observation, the amplitude of variability for salinity is strikingly smaller compared to PS89. The salinity values for PS117 range only between 34.13 and 34.29, while they range between 34.03 and 34.34 for PS89. With values between -1.58 °C (at the surface) and near freezing -1.89 °C (at the bottom), the temperatures measured during PS117 have a smaller range and are generally lower than those measured for PS89 (-1.42 to -1.85 °C). In contrast to PS89, no mixed layer was identified at any point during the PS117 tidal period, as a steep density gradient was absent and the entire water column was better mixed.

3.3 Biogeochemical variability

Despite the lower vertical resolution, the discrete bottle measurements capture the variability in the water column well, as shown by comparing the discrete bottle and continuous profile measurements for density (Fig. E1). We are therefore confident that the discrete biogeochemical measurements are also representative of the variability in the water column at the time of sampling.

The DIC and TA content mimic the tidal signature as seen for salinity (Fig. 4): their content decreases throughout the water column when the tide comes in, and increases as the tide goes out. The variability is, again, much lower during PS117 than during PS89. For the PS89 tidal observation, the DIC (TA) varied between 2174.3 and 2217.9 μmol kg^{-1} (2307.3 and 2327.1 μmol kg^{-1}) at the surface (<50 m) and between 2186.8 and 2222.7 μmol kg^{-1} (2312.3 and 2328.7 μmol kg^{-1}) at greater depths (>50 m). During PS117, DIC and TA content overall ranged between 2202.6 - 2220.1 μmol kg^{-1} and 2311.5 - 2322.3 μmol kg^{-1}, respectively. Salinity-normalised DIC (nDIC) and TA (nTA) profiles (according to Friis et al., 2003) lose much of the semi-diurnal variability, suggesting that physical processes, such as advection and mixing, are the dominant drivers of the observed variability (Fig. G1). PS117 nDIC values are markedly higher than those for most PS89 samples (Fig. 5). A part of this increase in nDIC over time could be result of the increase in atmospheric CO_2, assuming at least partial equilibration with the atmosphere.

PS117 nitrate (28.9 - 30.1 μmol kg^{-1}), phosphate (2.0 - 2.1 μmol kg^{-1}), and dissolved oxygen (322.0 - 333.2 μmol kg^{-1}) concentrations throughout the water column have similar values as those at the bottom of the water column during PS89 (Fig.

https://doi.org/10.5194/os-2022-19
Preprint. Discussion started: 1 April 2022

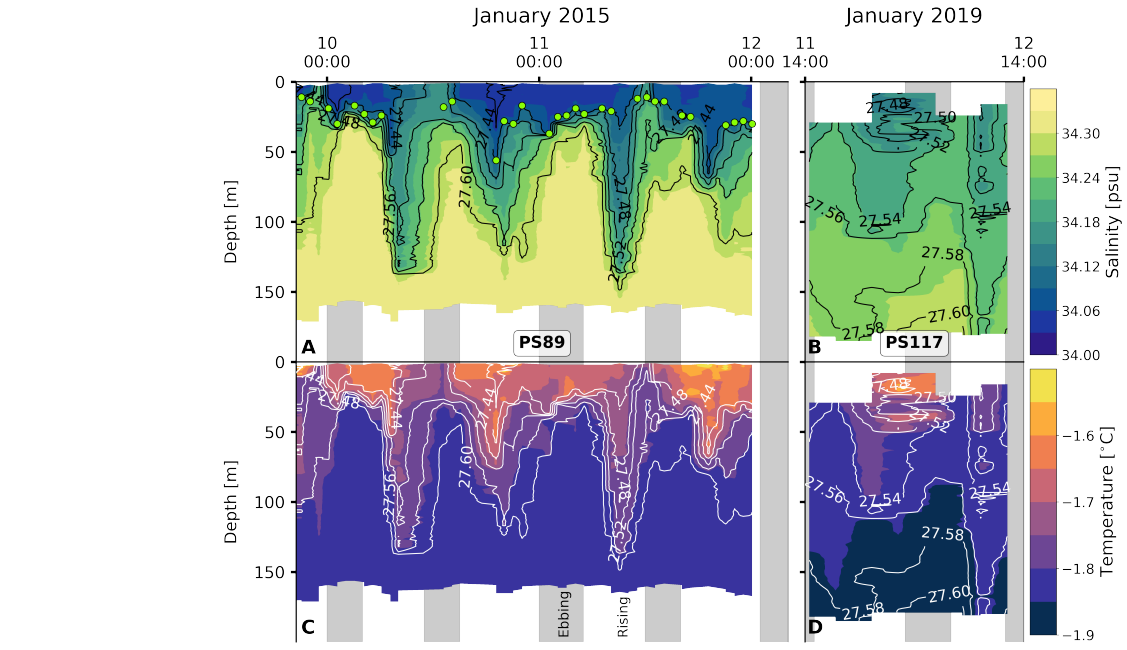

Figure 3. A, B) Salinity for PS89 and PS117, respectively. Green markers in A indicate the mixed layer depth (MLD) for casts where a mixed layer could clearly be identified according to a strong density gradient. MLD is identified as the depth at which the density difference with the average density values in the top 10 m is 0.02 kg m^{-3}. Temperature profiles are shown in C (PS89) and D (PS117). White contour lines represent isopycnals in kg m^{-3}. Vertical grey-coloured areas indicate times of ebbing tide.

6, G2, G4). Fluorescence was barely detected during PS117 (Fig. 6). Silicate has an offset between both case studies (Fig. G6). The silicate concentration is also relatively uniform in the water column during PS117 (58.3 - 59.8 μmol kg^{-1}; Fig. G2). Instead of values close to the upper part of the PS89 silicate range (as is the case for nitrate and phosphate), the PS117 silicate values lie around the mean silicate values measured for PS89 (60.0 $\pm$ 1.1 μmol kg^{-1}; Fig. G4). Whereas the salinity-normalised concentrations for nitrate and phosphate during PS117 have an average that is significantly higher (29.7 $\pm$ 0.1 μmol kg^{-1} and 2.0 $\pm$ 0.01μmol kg^{-1}, respectively) than those for PS89 (28.1 $\pm$ 0.3 μmol kg^{-1} and 1.9 $\pm$ 0.04 μmol kg^{-1}), the salinity-normalised silicate averages are similar (59.5 $\pm$ 0.5 μmol kg^{-1} for PS89 and 59.2 $\pm$ 0.2 μmol kg^{-1} for PS117; Fig. G5).

4 Discussion

4.1 Water masses and biogeochemistry

Hydrographically, the water measured during both tidal observations is identified as Eastern Shelf Water (ESW), which is found south of the Antarctic Slope Front (ASF) where pycnoclines slope downwards towards the south at the edge of the narrow continental shelf of the Dronning Maud Land coastline (Heywood et al., 1998). ESW is characterised by salinities

https://doi.org/10.5194/os-2022-19
Preprint. Discussion started: 1 April 2022

Ocean Science
Discussions
Open Access
EGU

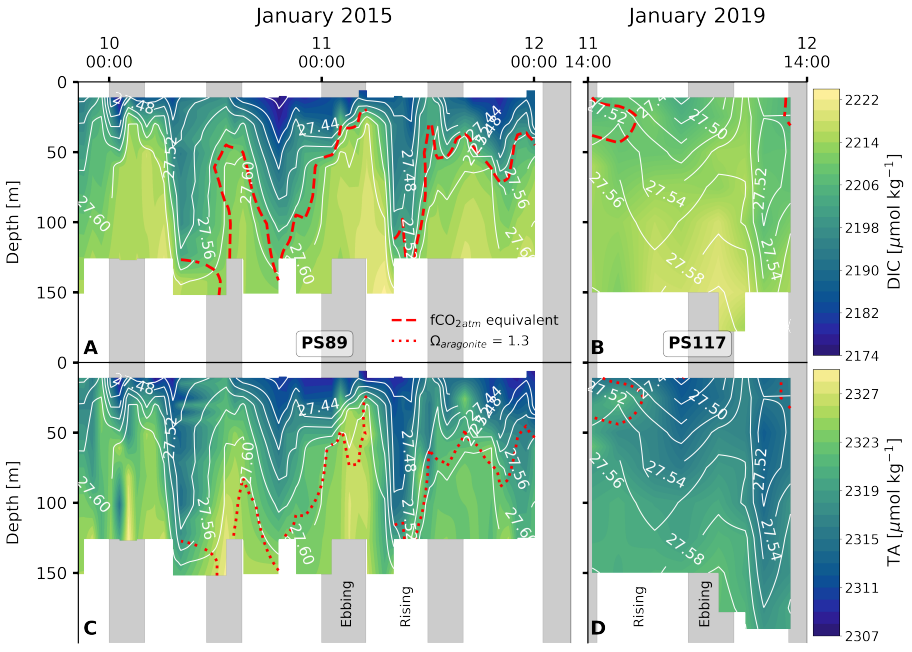

Figure 4. DIC content at the sampling site during the PS89 (A) and PS117 (B) tidal observations. TA content for the PS89 (C) and PS117 (D) observations. White contour lines indicate sigma-t in kg m^{-3}. Vertical grey shaded areas indicate periods of ebbing tide, as defined in the text. Red dashed line represents the depth at which the seawater fCO_2 is equal to the atmospheric fCO_2, which is 377 μatm in January 2015 and 387 μatm in January 2019. Seawater shallower than this depth is undersaturated in fCO_2 compared to the atmosphere. For PS117 (B), the seawater is mostly oversaturated in fCO_2 compared to the atmosphere. The red dotted line represents the depth at which the seawater pH = 8.05.

between 34.28 and 34.4 and temperatures close to freezing point (Carmack, 1974). ESW itself is a mixture of the following (Fahrbach et al., 1994):

- Winter Water (WW, winter surface water capped by a warmer summer stratification; characterised by a subsurface temperature minimum (Nicholls et al., 2009))
- Antarctic Surface Water (AASW, derived from WW that has been freshened by sea ice melt and heated by solar radiation in the spring and summer)
- modified Warm Deep Water (mWDW, which is the result of mixing between WW and WDW along the ASF (Ryan et al., 2020))
- glacial melt water (GMW, induced by intrusions of warmer water, such as mWDW and AASW, underneath the ice shelf (Fahrbach et al., 1994; Zhou et al., 2014)).

https://doi.org/10.5194/os-2022-19
Preprint. Discussion started: 1 April 2022

Ocean Science
Discussions
Open Access
EGU

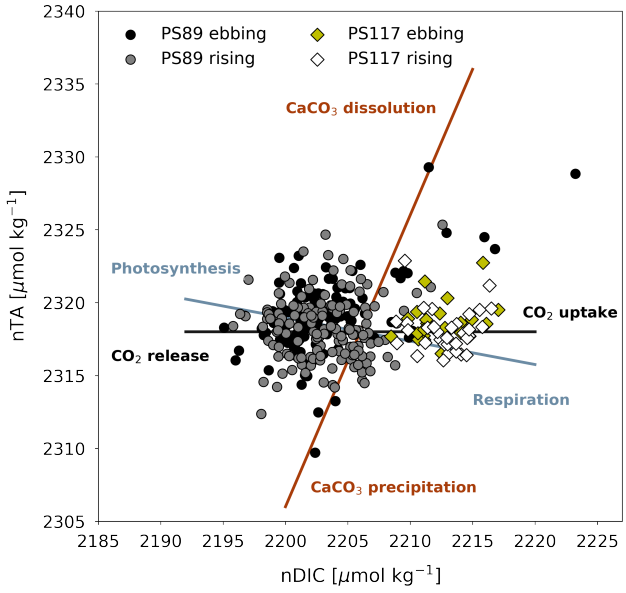

Figure 5. Salinity-normalised TA (nTA) and DIC (nDIC) plotted against each other for PS89 (circles) and PS117 (diamonds) tidal data. Samples collected during or ebbing (black circles and yellow diamonds) or rising tide (grey circles and white diamonds) are differentiated by different marker colours. Theoretical process lines are drawn for $CaCO_3$ dissolution/precipitation, photosynthesis/respiration, and CO_2 uptake/release.

However, the oscillations in the physical and biogeochemical properties induced by the incoming and outgoing tide suggests that the tide is enabling movement and possibly mixing of water masses, which is especially pronounced in the PS89 dataset (Fig. 3). While water in the Ekström polynya can broadly be categorised as one water mass (i.e. ESW) according to the physical properties, we will here explore the deepening and shoaling of the isopyncals, as well as the changing water physico-chemical properties.

At rising tides during PS89, the tide brings in water from the north-east that is fresher and warmer compared to the water present at the sampling location during low tide (Fig. 3 A, C). A well-defined mixed layer with relatively uniform properties is seen at the surface during ebbing tide ($\sim$ 20 m depth), which tends to disappear or deepen when the tide comes in and the water column density decreases. Similar observations in tide-driven shoaling and deepening of isopycnals have been made in other Antarctic coastal systems, although in lower wind conditions (Llanillo et al., 2019, $<$4 m s^{-1}). A destabilising (stabilising) water column has previously been associated with the rising (ebbing) tide observed in coastal polynyas in the Arctic (Skogseth et al., 2013). In the latter study, the tidal variability was characterised by a cold salinity front that moved back and forth with the tide.

In our case study, the input of fresher water with lower DIC and TA content is likely advection of AASW from the north-east of the front (and sampling site), influenced by the summer sea ice melt. In addition to a dilution effect, the accompanying increased fluorescence signal during rising tide on PS89 suggests that photosynthesis in this water has likely contributed to its

https://doi.org/10.5194/os-2022-19
Preprint. Discussion started: 1 April 2022

Ocean Science
Discussions
Open Access
EGU

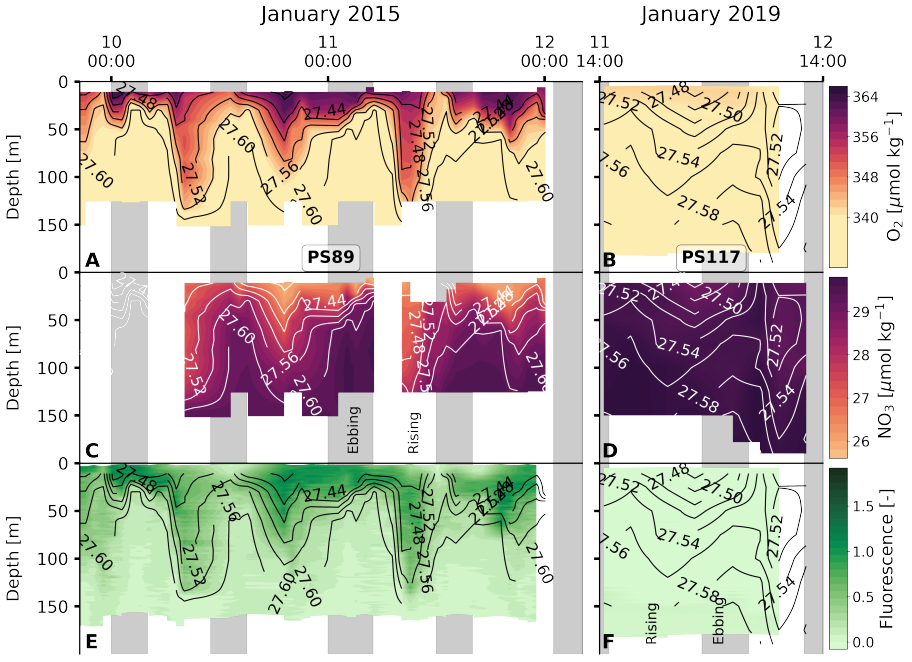

Figure 6. Same as Fig. 4, but for dissolved O_2, NO_3^-, and fluorescence.

lower DIC, TA, and nutrient content (Fig. 4, 6), which is sustained by solar radiation. The advection of fresher, lower DIC and TA sea water from the north-east during rising tide is likely enhanced by high winds (4 - 16 m s^{-1}) that consistently came from the north-east during - and in the week prior to - the PS89 tidal observation (Fig. H1A and H2A).

In comparison to PS89, the sampling site during PS117 has less pronounced freshening of the surface water during rising tide, thereby highlighting the interannual variability of the system. Instead, the entire water column is much more uniform with very few vertical gradients during the observation period. Differences in shape and size of the polynya between the two case studies may have affected the proximity of a salinity front to the sampling site. Even though the average sea ice concentration in the immediate vicinity of the sampling site was highly variable in the two months leading up to both PS89 and PS117 (not shown), the polynya was at least three times larger and more well-defined during PS117 than during PS89 (Section 2.1, Fig. A1 and A3). If a salinity front existed during PS117, it may have been located further away from the sampling site and closer to the sea ice edge of the polynya. Moreover, winds during PS117 may not have had the same enhancing effect on the advection of fresher, diluted water during rising tide compared to PS89. Whereas high winds during PS89 consistently came from the north-east, the wind speeds during PS117 were lower (3 - 10 m $^{-1}$) and their direction was more variable, mainly coming from the ice shelf side in the south-east (Fig. H1B and H2B). Modulating effects of winds on tidally-induced changes in physical water column properties, whether enhancing or counter-balancing, have also been observed in coastal systems at the Antarctic Peninsula (Llanillo et al., 2019).

https://doi.org/10.5194/os-2022-19
Preprint. Discussion started: 1 April 2022

The other side of the front (i.e from the south-west) brings in higher salinity and lower temperatures into the polynya during ebbing tide. This water seems less ventilated than AASW and shares physical properties with ice shelf water. Ice shelf water is characterised by potential temperatures of $<$-1.8 °C and salinity $>$34.6 (Carmack, 1974). However, recent work by Smith et al. (2020a) has shown that the temperature and salinity from a number of CTD profile measurements underneath the Ekström Ice Shelf in the same summer season as PS117 (2018/2019) ranged from -2.08 to -1.83 °C and 34.21 to 34.38, respectively (Fig. 7). These values overlap with the temperature and salinity at the bottom of the sampling site during both tidal observations, especially when the tide goes out. In terms of biogeochemical properties, the sub-ice shelf water is expected to be less ventilated compared to the AASW and to have relatively higher nutrient and DIC content, and lower dissolved oxygen content, as a result of net remineralisation (Fig. 4, 6).

It is possible that the ebbing tide draws out water from underneath the ice shelf which is expected to be colder. Indeed, the study by Smith et al. (2020a) attributed variability in two repeat profiles at one of the drill sites (EIS-4) to tidal influences extending underneath the ice shelf. As well as some vertical displacement of the ice shelf by the tidal force (Legrésy et al., 2004), horizontal displacement also occurs underneath the ice shelf. Another study found 12-hourly and 14-day fluctuations in a temperature time series underneath the Ekström Ice Shelf (June 2012 to February 2013), ranging between -1.94 and -1.6 $°C$ (Hoppmann et al., 2015). It also described effects of the tide on the glacial melt water outflow, which could be seen in the orientation and growth of platelet ice crystals in Atka Bay (Hoppmann et al., 2015), adjacent to the Ekström Ice Shelf and east of the sampling site in the current study. It therefore seems feasible that less ventilated water from underneath the ice shelf with lower oxygen and higher nutrient and DIC content can extend to the edge of the ice shelf during ebbing tide and into the polynya.

Even though mWDW is a source for eastern shelf water (Nicholls et al., 2009), we do not see a direct signal of mWDW in our dataset. The bathymetry of the cavity underneath the Ekström Ice Shelf slopes from about 450 m depth at the ice shelf edge to a maximum depth of 1100 m southwards towards the grounding-line (Smith et al., 2020a). Although troughs sculpted into the cavity's bathymetry (Smith et al., 2020a) potentially allow WDW (or its modified form) to enter it (Fahrbach et al., 1994) (a process that may be enhanced by tides), the warmer water is usually restricted to the north of the continental shelf in this region by prevailing easterly winds (Heywood et al., 1998; Thompson et al., 2018). The cavity is instead likely influenced by ESW that enters through Ekman transport (Zhou et al., 2014) of which a thin layer along the base of the ice shelf is colder and more buoyant, indicating outflows of ice shelf melt water (Smith et al., 2020a) (Fig. 7). Influence from ice shelf water seems to dominate the water properties in front of the ice shelf during PS117, despite the tides, which may be explained by the variable wind direction from the south-east (Fig. H2B) and potentially a large distance between a salinity front and the sampling site. In contrast, winds from the north-east enhance the influence of fresher, more ventilated ESW during PS89, and the sea ice conditions may have led to a salinity front that is closer to the sampling site.

The nDIC and nTA results indicate that most of the variability observed in this short time series is due to the physical movement of water masses by the tidal current, rather than biogeochemical processes happening *in situ* (Fig. G1). Net transport away from the ice shelf could create a tidally-driven horizontal DIC pump, whereby the sub-ice shelf water is a source of DIC that is transported away from the ice shelf into surface waters where it is exposed to the sea ice and the atmosphere. These

https://doi.org/10.5194/os-2022-19
Preprint. Discussion started: 1 April 2022

conditions are supportive of biomass production, which will decrease the DIC content only if the biological carbon uptake is more efficient than the advection of higher DIC waters. However, when we calculate the trajectory of a water parcel using the ship's position as a starting point and the average current velocity of the water column, the net transport is south/south-east, i.e. towards the ice shelf (not shown). This implies that the surface waters could be modifying the water underneath the ice shelf over time. The advection of lower DIC and salinity water might dilute the DIC content, but respiration of organic material might increase it over longer time periods. However, the total DIC content in the water column does not show a trend over time in this dataset and the net change in DIC content over six hour periods (including ebbing and rising tide) is zero (Fig. G3 for PS89). Our observations are a snapshot of a highly dynamic system and consequently we cannot analyse such modifications of the water physico-chemical properties with this dataset.

Variability in the salinity-normalised DIC and TA content could be the result of variable sea ice cover affecting photosynthesis by modified light availability and mixing of phytoplankton cells into deeper water during rising tide (Gleitz et al., 1994), $CaCO_3$ dissolution (Fig. 5), temperature changes affecting CO_2 solubility, and possible nutrient replenishment during ebbing tide. Yet, none of these processes seem particularly dominant or persistent in the nTA:nDIC ratio (Fig. 5). The results in Fig.5 show a legacy of processes that may have occurred in the past weeks to months, as the carbonate chemistry system's equilibration time with the atmosphere is slow, especially in sea ice covered regions. Additionally, this data might also reflect processes that happened in the sea ice, which will have affected the carbonate chemistry of the sea ice melt water and thus the properties of the AASW. While we here consider the tides to transport a salinity front back and forth across the sampling site, we must also recognise that the sampled mass of water on each side of the front is not exactly the same during each tidal phase, which contributes to the variability seen in the data.

Coastal polynyas have been described as "the most productive waters in the Southern Ocean" (Arrigo et al., 2015). Their chlorophyll *a* levels are found to peak in January, roughly coinciding with the peak of coastal polynyas' area of open water (Arrigo et al., 2015). In polynyas around Antarctica, iron supplied by basal melting is a major contributing factor to the variability in phytoplankton biomass (Arrigo et al., 2015). Considering that the observations in the current study were made in a coastal polynya of variable size directly adjacent to the Ekström Ice Shelf with an estimated basal melt rate of 4.2 Gt year^{-1} (Rignot et al., 2013), the lack of observable *in situ* nutrient and inorganic carbon uptake by primary productivity at the surface is perhaps unexpected. Tidal mixing that replenishes nutrients at the surface has been described to drive phytoplankton productivity in other tidal regions (Rogachev et al., 2001). However, primary productivity and its peak in the summer has been shown to be highly variable among Antarctic coastal polynyas, and the most likely drivers of low primary productivity are increased MLD, light stability, and grazing pressure (Arrigo and van Dijken, 2003). These are likely highly relevant factors in our case study. High phytoplankton growth rates require water column stability that lasts several weeks (Gleitz et al., 1994), which is absent during the case studies presented here. Even during ebbing tide, when the water column stratifies at a shallower depth during PS89, the duration of stratification is too short to support substantial growth and primary production. In a study in the Amundsen Sea, stations close to the Pine Island Glacier were characterised by a deep MLD and low phytoplankton biomass and Chl *a* despite high dissolved Fe availability (Alderkamp et al., 2012), suggesting that upwelling of Fe-rich basal meltwater mixed the water at the ice shelf's edge (Alderkamp et al., 2012; Gerringa et al., 2012). Outflow and mixing of ice shelf melt

https://doi.org/10.5194/os-2022-19
Preprint. Discussion started: 1 April 2022

water might have been stronger during PS117 than PS89. The water at the bottom of the profile during PS117 indeed has a temperature and salinity that is more similar to the temperature and salinity measured near the base of the ice shelf (mean of top 350 m of the ice shelf CTD casts EIS4-8 (Smith et al., 2020a)). The water underneath the shelf is directly affected by basal melt. During PS89, the bottom water temperature and salinity values resembled more closely those deeper in the cavity (e.g. the mean of the water deeper than 350 m of the ice shelf CTD casts EIS4-8; Fig. 7).

While a tidal movement of a salinity front or gradient across the sampling site is a possible and realistic explanation for the oscillations observed in the water column, validating it would require physico-chemical profiles between the Ekström Ice Shelf and the edge of the continental shelf. Without them, other relevant physical processes, such as regional circulation, tidal straining, or mixing, cannot be excluded. For the same reason, the distance from the ice shelf at which the tidally-driven deepening and shoaling of the isolines (most clearly seen for PS89) can be observed remains uncertain. The distance will depend on the strength of the tidal current and would have to be investigated with repeat transects from the ice shelf towards the open ocean at various points in the tidal cycle. Other mediating factors, such as winds and internal tidal waves generated by uneven bathymetry, would have to be additionally considered (Llanillo et al., 2019). Moreover, tidal mixing may erode fronts and modify water masses (such as at the ice shelf edge or of the ESW) over time, adding a temporal dimension to the effect of the tide on the shelf waters in this region.

4.2 Air-sea CO_2 exchange

The tidally-induced variability in the water column implies that the timing of sampling matters when estimating the relative contribution of coastal regions to the total CO_2 flux of the Weddell Sea. We first present the variability in the CO_2 flux during the tidal observation periods. We then illustrate that bias can be introduced in our understanding of the relative importance of coastal regions along the Weddell Sea if sampling strategies do not take tidal influences into account.

The difference in the fCO_2 of the seawater and the atmosphere is what drives a positive or negative CO_2 flux at the air-sea interface. For the flux calculations, we used the average wind speed recorded during the PS89 and PS117 tidal observation periods: 10.7 and 6.6 m s^{-1}, respectively. This choice implies that the computed variability in the flux results is solely driven by the air-sea gradient of fCO_2. During the PS89 tidal observation period in January 2015, the surface water at the Ekström Ice Shelf was undersaturated in fCO_2 relative to the atmosphere (Fig. 4), creating a CO_2 sink (Fig. 8). However, the depth at which the fCO_2 of the seawater is equal to that of the atmosphere (marked by a dashed line in Fig. 4A) fluctuates between the bottom (incoming tide) and the surface (outgoing tide). Direct fCO_2 measurements were made using the vessel's underway system (at 11 m depth) during (as well as 2.5 days prior to the start of) the discrete seawater sampling, i.e. the start of the PS89 tidal observation period (Fig. D1). fCO_2 correlates very well with the salinity, again indicating that physical movement of water is the dominant driver of the variability. CO_2 fluxes determined from the underway measurements a) compare well with the fluxes calculated from the discrete seawater carbonate chemistry results where they overlap in time, and b) show an even more drastic fluctuation on the 7^{th} and 8^{th} of January 2015, when the flux status of the sampling site swung between a sink (rising tide) and a source (ebbing tide) of CO_2 twice within 24 hours (Fig. 8). This suggests that water with higher DIC

https://doi.org/10.5194/os-2022-19
Preprint. Discussion started: 1 April 2022

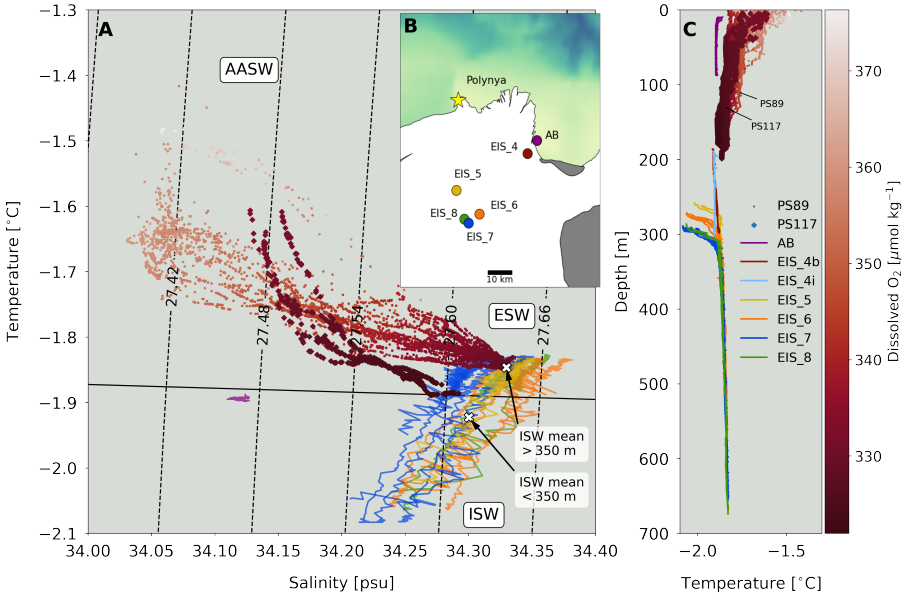

Figure 7. A) Temperature salinity diagram for PS89 (circles) and PS117 (diamonds) tidal observation periods, coloured according to dissolved oxygen concentrations, and the hot water drill CTD profiles through the ice shelf from Smith et al. (2020a) (coloured lines). Colours for hot water drill profiles correspond to the coloured marker locations on the map (B). AASW = Antarctic Surface Water, ESW = Eastern Shelf Water, ISW = Ice Shelf Water. The average temperature and salinity of water deeper and shallower than 350 m underneath the ice shelf are plotted as single purple markers. Contour lines indicate sigma-t in kg m^{-3}. Black line indicates freezing point at atmospheric pressure. C) Temperature profiles for PS89 (circles) and PS117 (diamonds) tidal observation periods, coloured according to oxygen concentrations, and the hot water drill CTD profiles underneath the ice shelf from Smith et al. (2020a).

content reached the surface during ebbing tide. The CO_2 sink during PS89 is as large as -19.9 mmol m^{-2} day^{-1}, while the largest CO_2 source reaches 6.9 mmol m^{-2} day^{-1} (Fig. 8).

During PS117, the entire water column has a higher fCO_2 than the atmospheric value, except for a patch between 50 and 20 m depth at the start and end of the tidal observation period (Fig. 4B). Even though not all PS117 CTD cast measurements started as shallow as those from PS89, the few casts that did have measurements starting <20 m showed a lack of a strong gradient in the DIC and TA content at the surface. The shallowest discrete carbonate chemistry water samples are therefore considered to be representative enough of the water properties at the surface. Accordingly, the site is likely to have been a small source of CO_2 at this time in January 2019. Using the fCO_2 results based on the discrete water sampling, the average CO_2 uptake during the PS89 tidal observation period is -8.0 $\pm$ 3.7 mmol m^{-2} day^{-1} ($\pm$ 1σ). For PS117, the average CO_2 release to the atmosphere is 1.4 $\pm$ 0.7 mmol m^{-2} day^{-1}. Even though the size of the coastal polynya was variable, the sampling site was free of sea ice during the tidal observations and it is assumed to have been ice free for the entire summer. We therefore have not scaled the gas transfer velocity with the fraction of open water area. At times during the summer when the site does get covered by sea ice, the amplitude of the CO_2 flux would be subdued.

https://doi.org/10.5194/os-2022-19
Preprint. Discussion started: 1 April 2022

The importance of strategic seawater sampling for the purpose of obtaining reliable air-sea gas exchange values in regions, such as the Ekström coastal polynya, is illustrated by the following. Assuming the scenario we know for the PS89 tidal observation period, if discrete water samples had unknowingly only been collected during ebbing tide (higher seawater fCO_2), the calculated CO_2 flux (0.6 mmol m^{-2} day^{-1}) would have underestimated the strength of the CO_2 uptake by the polynya by up to 108 %, compared to the average uptake (-8.0 mmol m^{-2} day^{-1}), i.e. actually mistaking it for a small source rather than a sink of CO_2. However, if samples had only been collected during times of rising tide (lower seawater fCO_2), the capacity of the polynya to take up CO_2 (-15.9 mmol m^{-2} day^{-1}) would have been overestimated by up to 98 %, compared to the average uptake value. Since the variability of the CO_2 flux during PS117 was much lower (a CO_2 release ranging between 0.2 - 2.2 mmol m^{-2} day^{-1}), samples collected at any time during this 24 hour period would have been relatively representative of this tidal observation period, but not necessarily of the month or the entire summer season.

We emphasise the potential misrepresentation of the role of coastal polynyas in the Weddell Sea CO_2 uptake if tidal influences are not accounted for using two extreme scenarios from the hypothetical case where samples are collected only during rising or ebbing tide of the PS89 tidal observation: samples are only taken at either peak rising tide or peak ebbing tide, which lead to an overestimation or underestimation of the CO_2 flux, respectively (see above). We constrain results and comparisons to the summertime, assume that all coastal polynyas in the south-eastern Weddell Sea are influenced by the same water masses present in the Ekström polynya during the PS89 tidal observation, and assume the same wind speed to highlight the role of the seawater fCO_2 variability. Using the total area of polynyas along the south-eastern Weddell Sea coastline in the summer of 49 $\times$ 10^3 km^2 (as estimated by Arrigo and van Dijken (2003)), the total CO_2 flux for all polynyas along the south-eastern coastline would be -0.78 $\times 10^9$ mol day^{-1} (net CO_2 uptake), if data had only been collected during rising tide. It would have been 0.03 $\times 10^9$ mol day^{-1} (net CO_2 release), if data had only been collected during ebbing tide.

Brown et al. (2015) estimated a summer marine uptake of CO_2 for the entire Weddell Sea of -0.044 to -0.058 $\pm$ 0.010 Pg C yr^{-1}, based on a summertime ocean inversion. In our hypothetical, biased upscaling case of collecting carbonate chemistry samples during ebbing tide, we would determine that the contribution of eastern shelf polynyas to Brown et al.'s upper summer CO_2 uptake estimate is 0.2 % (using the same area for the Weddell Sea: 6.2 $\times$ 10^{12} m^2 and scaling the daily flux up to the whole year). If seawater samples had only been collected during rising tide, the contribution of the eastern shelf polynyas would have been estimated at 5.9 % to the total summer CO_2 uptake of the Weddell Sea. This is quite substantial considering that the area used here for the south-eastern coastal polynyas is less than 0.8 % of the total Weddell Sea area (including regions covered and not covered by sea ice). If the average CO_2 flux of PS89 had been used in this simplistic upscaling exercise instead of the extreme high- and low-end scenarios, then the total CO_2 flux of all Weddell Sea coastal polynyas would be -0.4 $\pm$ 0.18 $\times 10^9$ mol day^{-1} (3.0 % of Weddell Sea flux) for January 2015. There is an order of magnitude difference if the same upscaling exercise is done with the average flux for the PS117 experiment: 0.07 $\pm$ 0.034 $\times 10^9$ mol day^{-1} (0.5 % of Weddell Sea flux).

The above exercise is simply to highlight the variability in these coastal systems. Given both the scarcity of data in these regions and the challenges in reaching them, tides may be an important aspect to consider to explain some of the variability seen in previous and future oceanographic data. Although the Weddell Sea is considered to be an - albeit small - annual net CO_2 sink (Hoppema et al., 1999; Bakker et al., 2008; Brown et al., 2015), its CO_2 uptake is sensitive to the balance of physical,

https://doi.org/10.5194/os-2022-19
Preprint. Discussion started: 1 April 2022

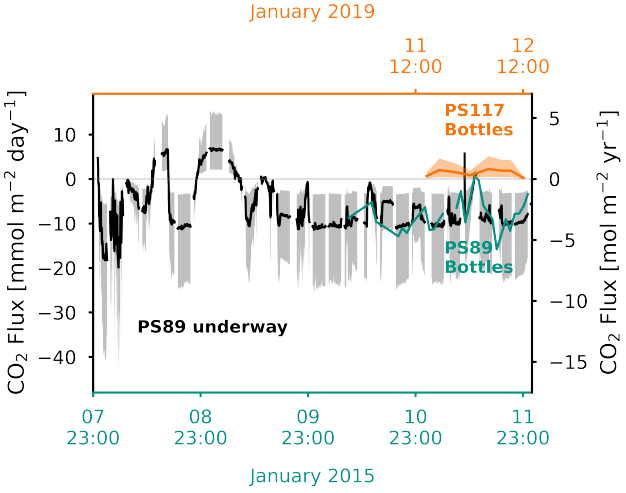

Figure 8. Air-sea CO_2 flux (in mmol $m^{-2}day^{-1}$ on the left y-axis and in mol $m^{-2}year^{-1}$ on the right y-axis) determined from the discrete surface seawater sample measurements for the PS89 (green) and PS117 (orange) tidal observation periods, and from the PS89 underway fCO_2 measurements (black), which started on the 7^{th} of January 2015. Dotted lines use the parameterisation by Sweeney et al. (2007), which was used in calculations by Brown et al. (2015). The filled shading indicates the range of the flux calculated using the minimum and maximum wind speed measured during PS89 and PS117, respectively. Negative flux represents CO_2 uptake by the ocean.

chemical, and biological processes, such as sea ice growth/melt, regional wind strength/patterns, circulation, and biological CO_2 drawdown (Brown et al., 2015). The coastal marine regions and the processes that govern their water properties may be equally sensitive and their changes on time-scales of hours to weeks or months may be mediated by the tides.

5 Conclusions

We present the significant semi-diurnal influence of tides on the water properties and carbonate chemistry at the margins of a coastal polynya hugging the Ekström Ice Shelf in the south-eastern Weddell Sea. Advection of lower DIC and TA waters from the north-east during rising tide influenced by sea ice melt, decreases the salinity and fCO_2 at the sampling site and results in CO_2 draw-down from the atmosphere. As the sampling site is located directly next to the ice shelf, it sees the extension of the water underneath the ice shelf, which is drawn out from underneath during ebbing tide. This water is less ventilated and has a higher DIC and TA content (and therefore a higher fCO_2) compared to the water to the north-east, which decreases the strength of the CO_2 sink and can even reverse it on a semi-diurnal time scale.

Differences in the variability between the two tidal observations between January 2015 and January 2019 suggests a complex interaction between timing of the tide, local and regional sea ice melt, polynya area, basal melt, and local forces, such as wind speed and direction. The datasets here are too small to explore the mediating effects of these processes. Longer tidal observations and repeats are required, along with measurements of micro-nutrients, carbonate chemistry, biological productivity, and

https://doi.org/10.5194/os-2022-19
Preprint. Discussion started: 1 April 2022

oxygen isotopes, to be able to constrain interacting processes. A better understanding of the carbonate chemistry of the water underneath the ice shelf - although challenging to obtain - would help understand the influence of this water during ebbing tide. The observations presented here were obtained from a stationary sampling site. Without knowing the hydrological conditions in the surrounding area at various time points in the tidal cycle, we must consider that our conclusions only apply to a very local area, the margins of polynyas, or the edges of ice shelves. Hydrographic transects between the ice shelf and out towards the edge of the continental shelf (across the polynya and underneath the sea ice) at ebbing and rising tide can help identify the extent to which the tidal oscillation, as seen in the case studies, is relevant further away from the coastline and from the polynya's margins. It may also help identify the formation and characteristics of - what is described here as - a salinity "front" that moves back and forth with the tide.

This case study has shown that tides can swing the status of coastal polynyas on the south-eastern continental shelf of the Weddell Sea from a strong sink to a source of CO_2 on a semi-diurnal time-scale. Seawater CO_2 uptake can be underestimated by 108 % and overestimated by 98 %, if these tidal changes are ignored. Awareness of the tidal impacts is required to implement strategic sampling techniques to obtain representative data in these extremely variable - and rarely accessible - systems that play a role in the sensitive balance of the Weddell Sea's net air-sea CO_2 exchange.

Data availability. For data access, contact the corresponding author. DIC and TA datasets will be made available online on the Pangaea database (in progress).

Appendix A: Sentinel images of Ekström polynya

https://doi.org/10.5194/os-2022-19
Preprint. Discussion started: 1 April 2022

Ocean Science
Discussions
Open Access
EGU

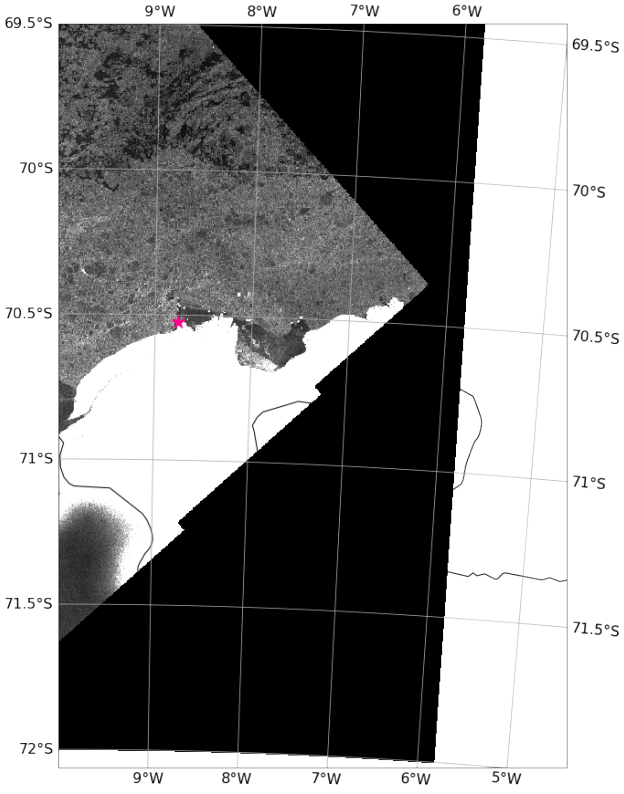

Figure A1. Sentinel-1 SAR image of the Ekström Ice Shelf and polynya on 12.01.2015 (PS89) (ESA, 2021).

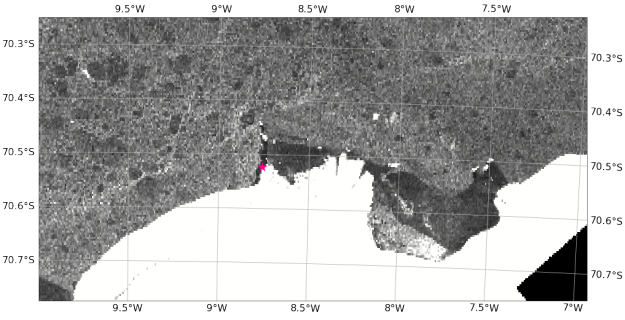

Figure A2. Sentinel-1 SAR image of the Ekström Ice Shelf and polynya on 12.01.2015 (PS89), zoomed in (ESA, 2021).

https://doi.org/10.5194/os-2022-19
Preprint. Discussion started: 1 April 2022

Ocean Science
Discussions
Open Access
EGU

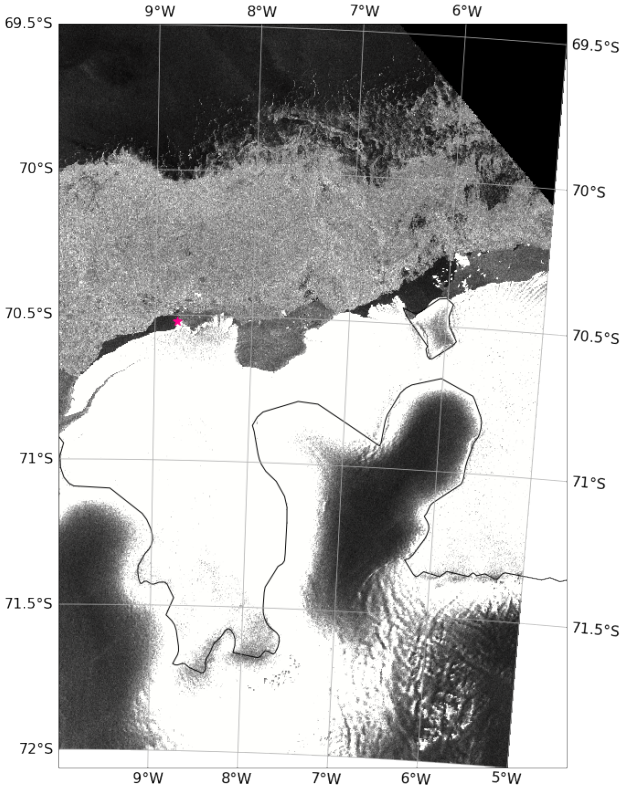

Figure A3. Sentinel-1 SAR image of the Ekström Ice Shelf and polynya on 10.01.2019 (PS117) (ESA, 2021).

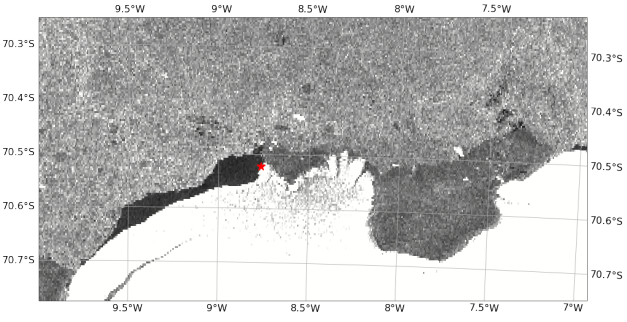

Figure A4. Sentinel-1 SAR image of the Ekström Ice Shelf and polynya on 10.01.2019 (PS117), zoomed in(ESA, 2021).

https://doi.org/10.5194/os-2022-19
Preprint. Discussion started: 1 April 2022

Table B1. References to all supporting data and data sources used in this work.

Data Type	Data Source	Reference
PS89 physical oceanographic data AWI CTD (continuous)	Pangaea	(Rohardt and Boebel, 2015a)
PS117 physical oceanographic data AWI CTD (continuous)	Pangaea	(Rohardt and Boebel, 2020)
PS89 CTD bottle data, incl. nutrient data (discrete)	Pangaea	(Rohardt and Boebel, 2015b)
PS117 CTD bottle data, incl. nutrient data (discrete)	Pangaea	(Rohardt et al., 2020)
PS89 ADCP	Pangaea	(Witte and Boebel, 2018)
PS117 ADCP	Pangaea	(Boebel and Tippenhauer, 2019)
PS89 wind speed	Pangaea	(König-Langlo, 2015)
PS117 wind speed	Pangaea	(Schmithüsen, 2020)
xCO_2 Syowa	ESRL NOAA	(Dlugokencky et al., 2019)
Antarctica boundaries	SCAR ADD	(Gerrish et al., 2020)
Ekström CTD data	Pangaea	(Smith et al., 2020b)
Sentinel 1 - SAR	European Space Agency	(ESA, 2021)

Appendix B: Data references

https://doi.org/10.5194/os-2022-19
Preprint. Discussion started: 1 April 2022

Ocean Science
Discussions
Open Access
EGU

Table C1. CTD sensor precisions.

Variable	Sensor or method	Expedition	Precision	Reference
Conductivity	SBE4c	PS89, manufacturer specification	0.003 mSc m^{-1} [a]	(Driemel et al., 2017)
Salinity	SBE4c	PS117	0.0004[b]	(Rohardt and Tippenhauer, 2020)
Temperature	SBE3plus	PS89, manufacturer specification	0.001 °C [a]	(Driemel et al., 2017)
Temperature	SBE3plus	PS117	0.00000 °C [a]	(Rohardt and Tippenhauer, 2020)
Pressure	Digiquartz with TC	PS89, manufacturer specification	0.015 % full scale	(Driemel et al., 2017)
Fluorescence	Wetlabs EcoFLR	PS89 and PS117	-	(Rohardt and Tippenhauer, 2020)
Dissolved O_2	SBE43	PS89	0.43[c] ml L^{-1}	(Boebel, 2015)
Dissolved O_2	SBE43	PS117	0.42[d] ml L^{-1}	(Rohardt and Tippenhauer, 2020)

[a] Average of the residual of post-calibration by Sea-Bird Scientific. [b] Standard deviation of the residual of the difference between the sensor measurements and the Optimare Precision Salinometer samples analysed on board. [c] Standard deviation of the difference in dissolved oxygen Winkler samples analysed on a potentiometric detection system and on a photometric end-point system on board. [d] Standard deviation of the residual of the difference between the sensor measurements and Winkler titration samples.

Table C2. Analytical uncertainty of the DIC and TA analyses using the variability of the CRM measurements per CRM batch. n refers to the number of CRMs that were run.

Dataset	CRM Batch No.	n	DIC [μmol kg^{-1}]		TA [μmol kg^{-1}]	
			CRM	Measured	CRM	Measured
PS89	137	25	2031.90 ± 0.62	2031.90 ± 1.22	2231.59 ± 0.32	2231.71 ± 1.09
PS117	176	133	2024.22 ± 0.82	2024.22 ± 3.32	2226.38 ± 0.53	2226.30 ± 3.18
PS117	185	17	2029.88 ± 0.62	2029.88 ± 2.88	2220.67 ± 0.58	2221.09 ± 0.85

Appendix C: Sampling at study site

https://doi.org/10.5194/os-2022-19
Preprint. Discussion started: 1 April 2022

Table C3. Analytical precisions for nutrient concentrations.

Dataset	NO_3^- [μmol kg^{-1}]	PO_4^{3-} [μmol kg^{-1}]	SiO_4 [μmol kg^{-1}]
PS89[a]	0.15	0.02	1.0
PS117[b]	0.041	0.008	0.057

[a] $\pm$ 1 σ of replicate samples for PS89. [b] $\pm$ 1 σ of repeat measurements of working standard at similar concentrations as average values for the tidal observation period of PS117: 30, 2, 60 μmol kg^{-1} for NO_3^-, PO_4^{3-}, and SiO_4, respectively.

https://doi.org/10.5194/os-2022-19
Preprint. Discussion started: 1 April 2022

Ocean Science
Discussions
Open Access
EGU

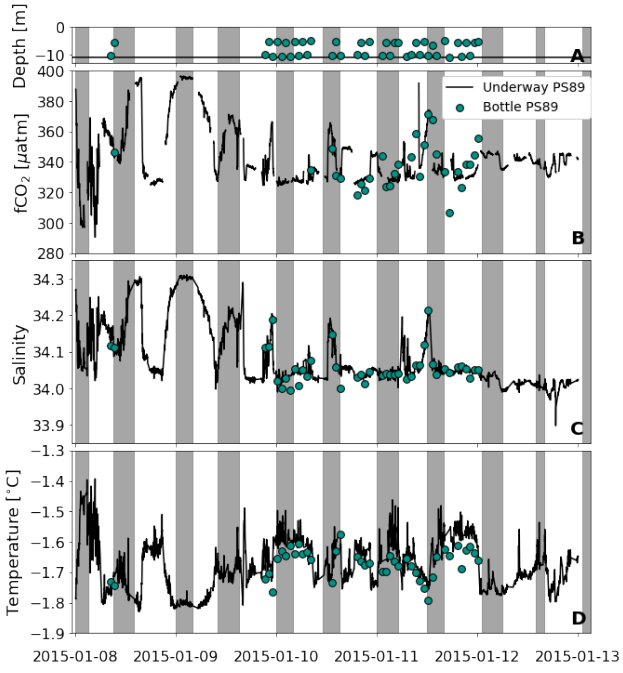

Figure D1. A comparison of measurements between the continuous measurements from the on-board underway system and the discrete samples of the surface seawater for PS89. A) Depth at which the surface discrete samples were collected during the tidal observation. The horizontal black line indicates depth at 11 m, which is the depth of the intake for the continuous fCO_2 measurements. B) The fCO_2 continuous measurements from the on-board underway system (black line) and the calculated fCO_2 from the discrete surface samples (circles). C) Same as B), but for temperature. D) Same as B), but for salinity. The grey areas indicate periods of ebbing tide (where the u and v components of the modelled tidal currents are both positive).

Appendix D: Underway measurements

https://doi.org/10.5194/os-2022-19
Preprint. Discussion started: 1 April 2022

Ocean Science
Discussions
Open Access
EGU

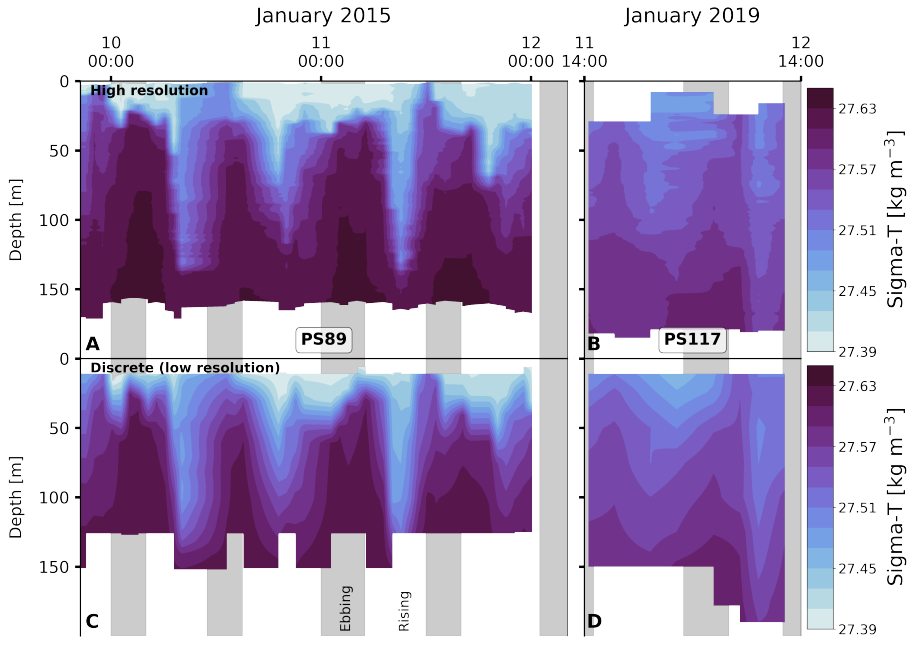

Figure E1. A) High vertical resolution profile sigma-t measurements for PS89. B) High vertical resolution profile sigma-t measurements for PS117. C) Discrete (low vertical resolution) profile measurements at bottle sampling depth for PS89. D) Discrete (low vertical resolution) profile measurements at bottle sampling depth for PS117.

Appendix E: Continuous profile vs. discrete bottle density measurements

To study the tidal cycle, profile measurements from the CTD casts are interpolated over time and depth. The high vertical resolution profile measurements for salinity and temperature are collected at a 1 dbar resolution on the down-cast, which is higher than the resolution of the discrete bottle samples and measurements that are collected on the up-cast. Difference in resolution and natural variability in the water column result in a slight difference between the high vertical resolution profile (down-cast) and discrete (low vertical resolution) bottle measurements (up-cast) at equal depth. To ensure that the bottle data with the lower vertical resolution is sufficiently representative, we compare the time and depth-interpolated bottle data to the high vertical profile measurements interpolated over time for the physical variables. As an example, we show the comparison for density (Fig. E1). It shows that the resolution of the bottle data sufficiently captures the same features in the water column as seen in the high resolution profile data. The bottle measurements are therefore reliable for interpretation of the chemical variables. As the higher vertical resolution profile measurements capture more detail of the features in the water column, these are used for the time series interpolations wherever applicable.

https://doi.org/10.5194/os-2022-19
Preprint. Discussion started: 1 April 2022

Ocean Science
Discussions
Open Access
EGU

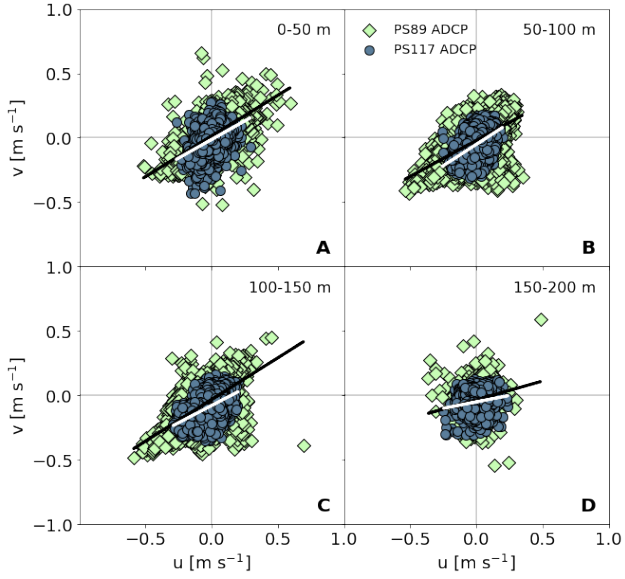

Figure F1. Correlations of the u and v components of the ADCP data for the tidal observations during PS89 (green diamonds) and PS117 (blue circles) between 0 - 50 m (A), 50 - 100 m (B), 100 - 150 m (C), and 150 - 200 m (D). All correlations are significant (p-value < 0.05) and positive, as shown with the black (PS89) and white (PS117) linear regression lines. A) $v = 0.63 \times u + 0.014$ (PS89); $v = 0.58 \times u$ - 0.01 (PS117). B) $v = 0.56 \times u$ - 0.02 (PS89); $v = 0.66 \times u$ - 0.05 (PS117). C) $v = 0.65 \times u$ - 0.03 (PS89); $v = 0.54 \times u$ - 0.08 (PS117). D) $v = 0.29 \times u$ - 0.034 (PS89); $v = 0.20 \times u$ - 0.05 (PS117).

Appendix F: Currents

https://doi.org/10.5194/os-2022-19
Preprint. Discussion started: 1 April 2022

Ocean Science
Discussions
Open Access
EGU

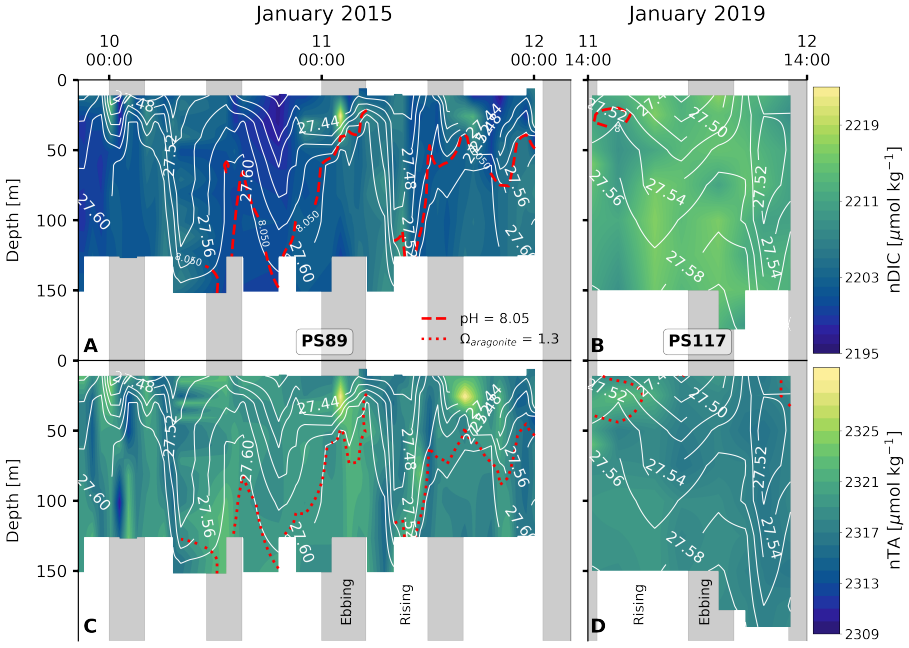

Figure G1. Salinity-normalised DIC content at the sampling site during the PS89 (A) and PS117 (B) tidal observations, as well as salinity-normalised TA content for the PS89 (C) and PS117 (D) observations. White contour lines indicate sigma-t in kg m^{-3}. Vertical grey shaded areas indicate periods of ebbing tide, as defined in the text. Dashed red lines indicate the depth at which the pH = 8.05. Dotted red lines indicate the depth at which the aragonite saturation state = 1.3. These are arbitrary values, to illustrate the variability in the water column.

Appendix G: Tidal variability

https://doi.org/10.5194/os-2022-19
Preprint. Discussion started: 1 April 2022

Ocean Science
Discussions
Open Access
EGU

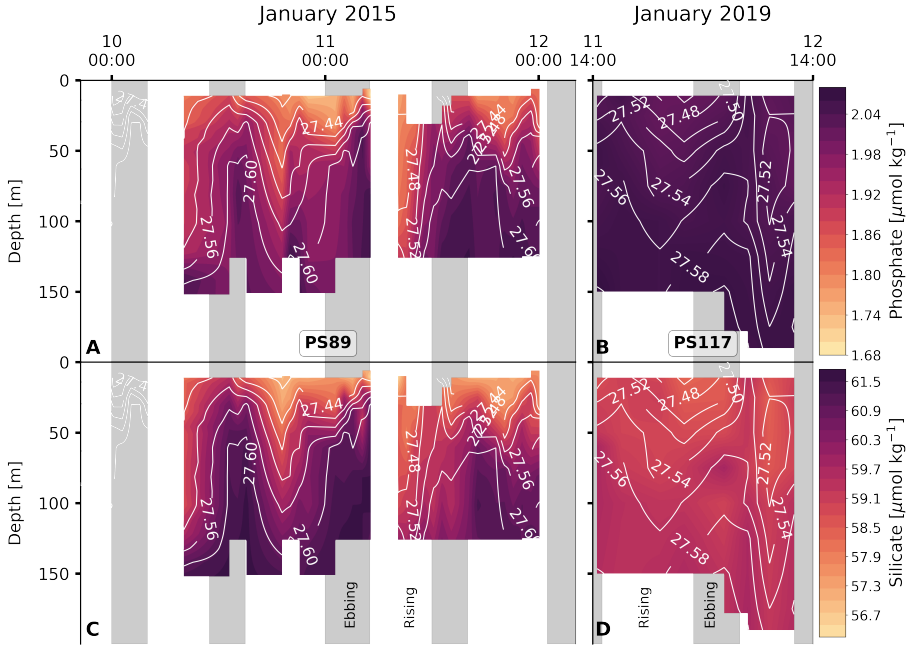

Figure G2. As for G1, for phosphate and silicate (excluding the pH and calcite saturation contours).

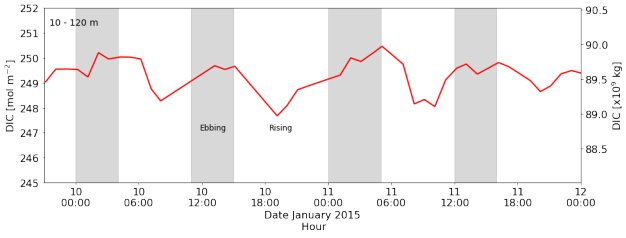

Figure G3. Left y axis: total water column DIC content between 10 and 120 m during the PS89 tidal observation. Right y axis: total DIC content between 10 and 120 m for the entire PS89 polynya, using the estimated dimensions in the text and assuming an ellipsoidal area.

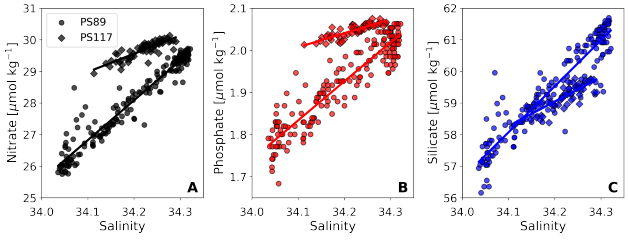

Figure G4. Nitrate (black), phosphate (red), and silicate (blue) content plotted against salinity for the PS89 (circles) and PS117 (diamonds) tidal observations, including linear regression lines.

https://doi.org/10.5194/os-2022-19
Preprint. Discussion started: 1 April 2022

Ocean Science
Discussions
Open Access
EGU

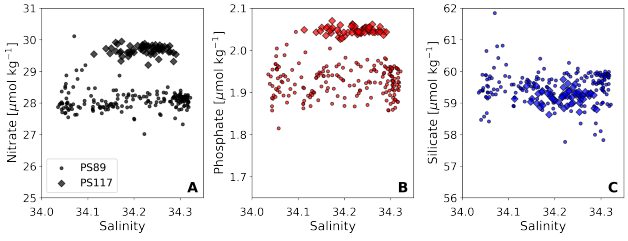

Figure G5. Salinity-normalised (following Friis et al. (2003)) nitrate (black), phosphate (red), and silicate (blue) content plotted against salinity for the PS89 (circles) and PS117 (diamonds) tidal observations.

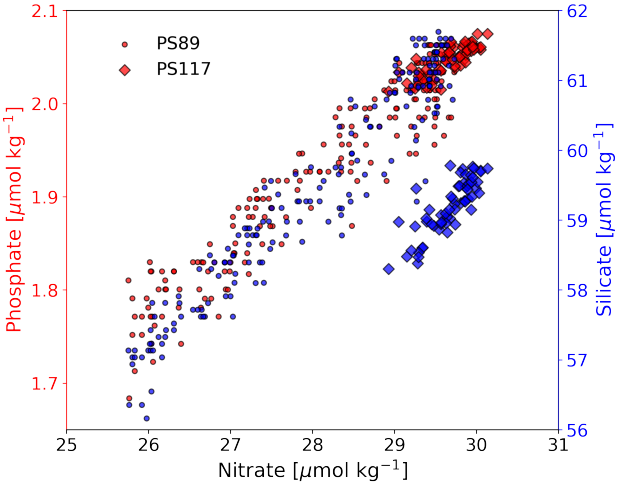

Figure G6. Phosphate (red) and silicate (blue) concentrations plotted against nitrate concentrations for the PS89 (circles) and PS117 (diamonds) tidal observations.

https://doi.org/10.5194/os-2022-19
Preprint. Discussion started: 1 April 2022

Ocean Science
Discussions
Open Access
EGU

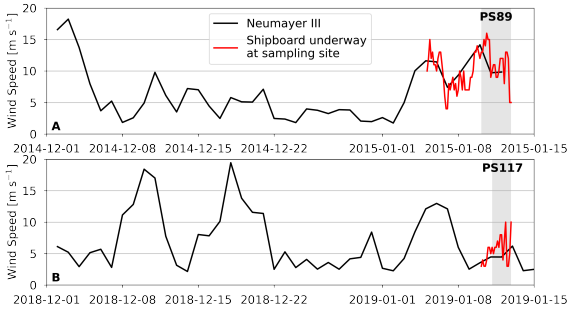

Figure H1. A) Wind speed measured at Neumayer III Research Station in the time prior and during the PS89 tidal observation, as well as the ship-board wind speed measurements during the PS89 tidal observation. B) Wind speed measured at Neumayer III Research Station in the time prior and during the PS117 tidal observation, as well as the ship-board wind speed measurements during the PS117 tidal observation. Grey areas indicate the duration of the tidal observations.

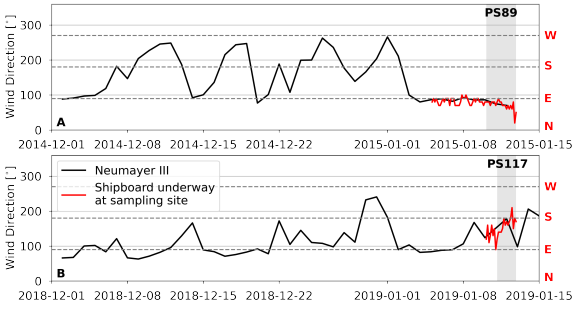

Figure H2. A) Wind direction measured at Neumayer III Research Station in the time prior and during the PS89 tidal observation, as well as the ship-board wind direction measurements during the PS89 tidal observation. B) Wind direction measured at Neumayer III Research Station in the time prior and during the PS117 tidal observation, as well as the ship-board wind direction measurements during the PS117 tidal observation. Grey areas indicate the duration of the tidal observations. Horizontal dashed lines indicate 90°, 180°, and 270°. North, East, South, and West directions are indicated by the red initials at the right side of the plots.

Appendix H: Wind

https://doi.org/10.5194/os-2022-19
Preprint. Discussion started: 1 April 2022

Author contributions. ESD developed the concept for this manuscript, led the writing process, and collected/analysed/processed the PS117 DIC and TA samples. DCEB, MH, GDO, BQ, HJV, MGD, and JMSC provided valuable input and guidance for the development of this work. MGD and JMSC independently collected/analysed/processed the PS89 DIC and TA samples. BQ processed the PS117 ADCP data. DS and SO collected/analysed/processed the PS89 and PS117 nutrient data, respectively. GR ran the tidal model. STK collected and analysed the Winkler O_2 samples for the calibration of the dissolved O_2 sensors on PS117. All authors contributed to the manuscript.

Competing interests. The authors declare that they have no conflict of interest.

Acknowledgements. ESD's work is supported by the Natural Environment Research Council (NERC) through the EnvEast Doctoral Training Partnership (NE/L002582/1). Work done by ESD and DCEB for the PS117 expedition was supported by funding from the NERC for the PICCOLO project (NE/P021395/1). Partial support to JMSC and MGD was received from EU FP7 project CARBOCHANGE (Grant agreement No. 264879) for the participation in the PS89 ANT-XXX/2 cruise. We would like to thank the crew and captains of *R.V. Polarstern* and the scientists for the PS89 and PS117 expeditions for the cooperation on board and the unforgettable experiences. A special thank you goes out to Salar Karam and Kirstin Schulz for their patient discussions and valuable insights on physical oceanography of the study site.

https://doi.org/10.5194/os-2022-19
Preprint. Discussion started: 1 April 2022

References

Alderkamp, A. C., Mills, M. M., van Dijken, G. L., Laan, P., Thuróczy, C. E., Gerringa, L. J., de Baar, H. J., Payne, C. D., Visser, R. J., Buma, A. G., and Arrigo, K. R.: Iron from melting glaciers fuels phytoplankton blooms in the Amundsen Sea (Southern Ocean): Phytoplankton characteristics and productivity, Deep-Sea Research Part II: Topical Studies in Oceanography, 71-76, 32–48, https://doi.org/10.1016/j.dsr2.2012.03.005, 2012.

Anderson, L. G., Holby, O., Lindegren, R., and Ohlson, M.: The transport of anthropogenic carbon dioxide into the Weddell Sea, Journal of Geophysical Research, 96, https://doi.org/10.1029/91jc01785, 1991.

Andersson, A. J. and MacKenzie, F. T.: Revisiting four scientific debates in ocean acidification research, Biogeosciences, 9, 893–905, https://doi.org/10.5194/bg-9-893-2012, 2012.

Arrigo, K. R. and van Dijken, G. L.: Phytoplankton dynamics within 37 Antarctic coastal polynya systems, Journal of Geophysical Research: Oceans, 108, https://doi.org/10.1029/2002jc001739, 2003.

Arrigo, K. R., van Dijken, G. L., and Strong, A. L.: Environmental controls of marine productivity hot spots around Antarctica, Journal of Geophysical Research: Oceans, 120, 5545–5565, https://doi.org/10.1002/2015JC010888, 2015.

Bakker, D. C., Hoppema, M., Schröder, M., Geibert, W., and De Baar, H. J.: A rapid transition from ice covered CO_2-rich waters to a biologically mediated CO_2 sink in the eastern Weddell Gyre, Biogeosciences, 5, 1373–1386, https://doi.org/10.5194/bg-5-1373-2008, 2008.

Barber, D. G. and Massom, R. A.: Chapter 1 The Role of Sea Ice in Arctic and Antarctic Polynyas, in: Elsevier Oceanography Series, vol. 74, chap. 1, pp. 1–54, https://doi.org/10.1016/S0422-9894(06)74001-6, 2007.

Boebel, O.: The expedition PS89 of the research vessel RV Polarstern to the Weddell Sea in 2014/2015, Berichte zur Polar-und Meeresforschung= Reports on polar and marine research, 689, https://doi.org/10.2312/BzPM_0689_2015, 2015.

Boebel, O.: The Expedition PS117 of the Research Vessel POLARSTERN to the Weddell Sea in 2018/2019, Berichte zur Polar-und Meeresforschung= Reports on polar and marine research, 732, https://doi.org/10.2312/BzPM_0732_2019, 2019.

Boebel, O. and Tippenhauer, S.: Raw data of continuous VM-ADCP (vessel-mounted Acoustic Doppler Current Profiler) profile during POLARSTERN cruise PS117, https://doi.org/10.1594/PANGAEA.902725, 2019.

Brown, P. J., Jullion, L., Landschützer, P., Bakker, D. C., Naveira Garabato, A. C., Meredith, M. P., Torres-Valdés, S., Watson, A. J., Hoppema, M., Loose, B., Jones, E. M., Telszewski, M., Jones, S. D., and Wanninkhof, R.: Carbon dynamics of the Weddell Gyre, Southern Ocean, Global Biogeochemical Cycles, 29, 288–306, https://doi.org/10.1002/2014GB005006, 2015.

Carmack, E. C.: A quantitative characterization of water masses in the Weddell sea during summer, Deep-Sea Research and Oceanographic Abstracts, 21, 431–443, https://doi.org/10.1016/0011-7471(74)90092-8, 1974.

Dickson, A. G., Sabine, C. L., and Christian, J. R.: Guide to Best Practices for Ocean CO_2 Measurements, North Pacific Marine Science Organization, www.pices.int, 2007.

Dlugokencky, E., Mund, J., Crotwell, A., Crotwell, M., and Thoning, K.: Atmospheric Carbon Dioxide Dry Air Mole Fractions from the NOAA ESRL Carbon Cycle Cooperative Global Air Sampling Network, 1968-2018, https://doi.org/https://doi.org/10.15138/wkgj-f215, version: 2019–07, 2019.

Dmitrenko, I. A., Kirillov, S. A., Bloshkina, E., and Lenn, Y. D.: Tide-induced vertical mixing in the Laptev Sea coastal polynya, Journal of Geophysical Research: Oceans, 117, 1–19, https://doi.org/10.1029/2011JC006966, 2012.

https://doi.org/10.5194/os-2022-19
Preprint. Discussion started: 1 April 2022

Driemel, A., Fahrbach, E., Rohardt, G., Beszczynska-Möller, A., Boetius, A., Budéus, G., Cisewski, B., Engbrodt, R., Gauger, S., Geibert, W., Geprägs, P., Gerdes, D., Gersonde, R., Gordon, A. L., Grobe, H., Hellmer, H. H., Isla, E., Jacobs, S. S., Janout, M., Jokat, W., Klages, M., Kuhn, G., Meincke, J., Ober, S., Østerhus, S., Peterson, R. G., Rabe, B., Rudels, B., Schauer, U., Schröder, M., Schumacher, S., Sieger, R., Sildam, J., Soltwedel, T., Stangeew, E., Stein, M., Strass, V. H., Thiede, J., Tippenhauer, S., Veth, C., Von Appen, W. J., Weirig, M. F., Wisotzki, A., Wolf-Gladrow, D. A., and Kanzow, T.: From pole to pole: 33 years of physical oceanography onboard R/V Polarstern, Earth System Science Data, 9, 211–220, https://doi.org/10.5194/essd-9-211-2017, 2017.

Eicken, H. and Lange, M. A.: Development and properties of sea ice in the coastal regime of the southeastern Weddell Sea, Journal of Geophysical Research: Oceans: Oceans, 94, 8193–8206, https://doi.org/10.1029/JC094iC06p08193, 1989.

ESA: Sentinel 1 SAR Dataset, european Space Agency. Data retrieved from Copernicus Open Access Hub: https://scihub.copernicus.eu/, 2021.

Fahrbach, E., Peterson, R. G., Rohardt, G., Schlosser, P., and Bayer, R.: Suppression of bottom water formation in the southeastern Weddell sea, Deep-Sea Research Part I, 41, 389–411, https://doi.org/10.1016/0967-0637(94)90010-8, 1994.

Friis, K., Körtzinger, A., and Wallace, D. W.: The salinity normalization of marine inorganic carbon chemistry data, Geophysical Research Letters, 30, 1–4, https://doi.org/10.1029/2002GL015898, 2003.

Gerringa, L. J., Alderkamp, A. C., Laan, P., Thuróczy, C. E., De Baar, H. J., Mills, M. M., van Dijken, G. L., van Haren, H., and Arrigo, K. R.: Iron from melting glaciers fuels the phytoplankton blooms in Amundsen Sea (Southern Ocean): Iron biogeochemistry, Deep-Sea Research Part II: Topical Studies in Oceanography, 71-76, 16–31, https://doi.org/10.1016/j.dsr2.2012.03.007, 2012.

Gerrish, L., Fretwell, P., and Cooper, P.: High resolution vector polygons of the Antarctic coastline (7.3) [Data set]., https://doi.org/10.5285/0a6d85d7-fc9c-4d68-a58d-e792f68ae9f4, 2020.

Gleitz, M., Bathmann, U. V., and Lochte, K.: Build-up and decline of summer phytoplankton biomass in the eastern Weddell Sea, Antarctica, Polar Biology, 14, 413–422, https://doi.org/10.1007/BF00240262, 1994.

Heywood, K. J., Locarnini, R. A., Frew, R. D., Dennis, P. F., and King, B. A.: Transport and water masses of the Antarctic slope front system in the eastern Weddell Sea, Ocean, ice, and atmosphere: Interactions at the Antarctic continental margin, Antarctic Research Series, 75, 203–214, 1998.

Ho, D. T., Law, C. S., Smith, M. J., Schlosser, P., Harvey, M., and Hill, P.: Measurements of air-sea gas exchange at high wind speeds in the Southern Ocean: Implications for global parameterizations, Geophysical Research Letters, 33, L16611, https://doi.org/10.1029/2006GL026817, 2006.

Hoppema, M. and Anderson, L. G.: Chapter 6 Biogeochemistry of Polynyas and Their Role in Sequestration of Anthropogenic Constituents, in: Elsevier Oceanography Series, vol. 74, chap. 6, pp. 193–221, https://doi.org/10.1016/S0422-9894(06)74006-5, 2007.

Hoppema, M., Fahrbach, E., Stoll, M. H., and De Baar, H. J.: Annual uptake of atmospheric CO_2 by the Weddell sea derived from a surface layer balance, including estimations of entrainment and new production, Journal of Marine Systems, 19, 219–233, https://doi.org/10.1016/S0924-7963(98)00091-8, 1999.

Hoppmann, M., Nicolaus, M., Paul, S., Hunkeler, P. A., Heinemann, G., Willmes, S., Timmermann, R., Boebel, O., Schmidt, T., Kühnel, M., König-Langlo, G., and Gerdes, R.: Ice platelets below Weddell Sea landfast sea ice, Annals of Glaciology, 56, 175–190, https://doi.org/10.3189/2015AoG69A678, 2015.

Huhn, O., Rhein, M., Hoppema, M., and van Heuven, S.: Decline of deep and bottom water ventilation and slowing down of anthropogenic carbon storage in the Weddell Sea, 1984-2011, Deep-Sea Research Part I: Oceanographic Research Papers, 76, 66–84, https://doi.org/10.1016/j.dsr.2013.01.005, 2013.

https://doi.org/10.5194/os-2022-19
Preprint. Discussion started: 1 April 2022

Humphreys, M. P. and Matthews, R. S.: Calkulate: total alkalinity from titration data in Python, https://doi.org/10.5281/zenodo.2634304, documentation: https://mphumphreys.wordpress.com/projects/software/calkulate/, 2022.

Humphreys, M. P., Lewis, E. R., Sharp, J. D., and Pierrot, D.: PyCO2SYS v1.8: Marine carbonate system calculations in Python, Geoscientific Model Development, 15, 15–43, https://doi.org/10.5194/gmd-15-15-2022, 2022.

Huot, P. V., Fichefet, T., Jourdain, N. C., Mathiot, P., Rousset, C., Kittel, C., and Fettweis, X.: Influence of ocean tides and ice shelves on ocean–ice interactions and dense shelf water formation in the D'Urville Sea, Antarctica, Ocean Modelling, 162, 101 794, https://doi.org/10.1016/j.ocemod.2021.101794, 2021.

Kirillov, S. A., Dmitrenko, I. A., Hölemann, J. A., Kassens, H., and Bloshkina, E.: The penetrative mixing in the Laptev Sea coastal polynya pycnocline layer, Continental Shelf Research, 63, 34–42, https://doi.org/10.1016/j.csr.2013.04.040, 2013.

König-Langlo, G.: Meteorological observations during POLARSTERN cruise PS89 (ANT-XXX/2), https://doi.org/10.1594/PANGAEA.844571, 2015.

Legrésy, B., Wendt, A., Tabacco, I., Rémy, F., and Dietrich, R.: Influence of tides and tidal current on Mertz Glacier, Antarctica, Journal of Glaciology, 50, 427–435, https://doi.org/10.3189/172756504781829828, 2004.

Lewis, E. and Wallace, D.: Program Developed for CO_2 System Calculations, Carbon Dioxide Information Analysis Center, 1998.

Llanillo, P. J., Aiken, C. M., Cordero, R. R., Damiani, A., Sepúlveda, E., and Fernández-Gómez, B.: Oceanographic Variability induced by Tides, the Intraseasonal Cycle and Warm Subsurface Water intrusions in Maxwell Bay, King George Island (West-Antarctica), Scientific Reports, 9, 1–17, https://doi.org/10.1038/s41598-019-54875-8, 2019.

Makinson, K., Holland, P. R., Jenkins, A., Nicholls, K. W., and Holland, D. M.: Influence of tides on melting and freezing beneath Filchner-Ronne Ice Shelf, Antarctica, Geophysical Research Letters, 38, 4–9, https://doi.org/10.1029/2010GL046462, 2011.

Mintrop, L.: VINDTA 3C Manual, https://www.marianda.com/, manual downloaded from https://www.marianda.com/, 2016.

Mueller, R. D., Hattermann, T., Howard, S. L., and Padman, L.: Tidal influences on a future evolution of the Filchner-Ronne Ice Shelf cavity in the Weddell Sea, Antarctica, Cryosphere, 12, 453–476, https://doi.org/10.5194/tc-12-453-2018, 2018.

Nicholls, K. W., Østerhus, S., Makinson, K., Gammelsrød, T., and Fahrbach, E.: Ice-ocean processes over the continental shelf of the Southern Weddell Sea, Antarctica: A review, Reviews of Geophysics, 47, 1–23, https://doi.org/10.1029/2007RG000250, 2009.

Orsi, A. H., Smethie, W. M., and Bullister, J. L.: On the total input of Antarctic waters to the deep ocean: A preliminary estimate from chlorofluorocarbon measurements, Journal of Geophysical Research: Oceans, 107, https://doi.org/10.1029/2001jc000976, 2002.

Padman, L., Fricker, H. A., Coleman, R., Howard, S., and Erofeeva, L.: A new tide model for the Antarctic ice shelves and seas, Annals of Glaciology, 34, 247–254, https://doi.org/10.3189/172756402781817752, 2002.

Padman, L., Howard, S. L., Orsi, A. H., and Muench, R. D.: Tides of the northwestern Ross Sea and their impact on dense outflows of Antarctic Bottom Water, Deep-Sea Research Part II: Topical Studies in Oceanography, 56, 818–834, https://doi.org/10.1016/j.dsr2.2008.10.026, 2009.

Padman, L., Siegfried, M. R., and Fricker, H. A.: Ocean Tide Influences on the Antarctic and Greenland Ice Sheets, Reviews of Geophysics, 56, 142–184, https://doi.org/10.1002/2016RG000546, 2018.

Renfrew, I. A.: Coastal polynyas in the southern Weddell Sea: Variability of the surface energy budget, Journal of Geophysical Research, 107, https://doi.org/10.1029/2000jc000720, 2002.

Rignot, E., Jacobs, S., Mouginot, J., and Scheuchl, B.: Ice-shelf melting around Antarctica, Science, 341, 266–270, https://doi.org/10.1126/science.1235798, 2013.

https://doi.org/10.5194/os-2022-19
Preprint. Discussion started: 1 April 2022

Rogachev, K. A., Carmack, E. C., Salomatin, A. S., and Alexanina, M. G.: Lunar fortnightly modulation of tidal mixing near Kashevarov Bank, Sea of Okhotsk, and its impacts on biota and sea ice, Progress in Oceanography, 49, 373–390, https://doi.org/10.1016/S0079-6611(01)00031-3, 2001.

Rohardt, G. and Boebel, O.: Physical oceanography during POLARSTERN cruise PS89 (ANT-XXX/2), https://doi.org/10.1594/PANGAEA.846701, 2015a.

Rohardt, G. and Boebel, O.: Physical oceanography measured on water bottle samples during POLARSTERN cruise PS89 (ANT-XXX/2), https://doi.org/10.1594/PANGAEA.846773, 2015b.

Rohardt, G. and Boebel, O.: Physical oceanography during POLARSTERN cruise PS117, https://doi.org/10.1594/PANGAEA.910663, 2020.

Rohardt, G. and Tippenhauer, S.: CTD Data Processing Report RV POLARSTERN Cruise PS117, https://doi.org/10.1594/PANGAEA.910663, 2020.

Rohardt, G., Middag, R., Boebel, O., Trace-Kleeberg, S., and Ossebaar, S.: Physical oceanography measured on water bottle samples during POLARSTERN cruise PS117, https://doi.org/10.1594/PANGAEA.910673, 2020.

Ryan, S., Hellmer, H. H., Janout, M., Darelius, E., Vignes, L., and Schröder, M.: Exceptionally Warm and Prolonged Flow of Warm Deep Water Toward the Filchner-Ronne Ice Shelf in 2017, Geophysical Research Letters, 47, https://doi.org/10.1029/2020GL088119, 2020.

Schmithüsen, H.: Meteorological observations during POLARSTERN cruise PS117, https://doi.org/10.1594/PANGAEA.913632, 2020.

Sims, R. P., Bedington, M., Schuster, U., Watson, A., Kitidis, V., Torres, R., Findlay, H., Fishwick, J., Brown, I., and Bell, T.: Tidal mixing of estuarine and coastal waters in the Western English Channel controls spatial and temporal variability in seawater CO_2, Biogeosciences Discussions, 19, 1657–1674, https://doi.org/10.5194/bg-19-1657-2022, 2022.

Skogseth, R., McPhee, M. G., Nilsen, F., and Smedsrud, L. H.: Creation and tidal advection of a cold salinity front in Storfjorden: 1. Polynya dynamics, Journal of Geophysical Research: Oceans, 118, 3278–3291, https://doi.org/10.1002/jgrc.20231, 2013.

Smith, E. C., Hattermann, T., Kuhn, G., Gaedicke, C., Berger, S., Drews, R., Ehlers, T. A., Franke, D., Gromig, R., Hofstede, C., Lambrecht, A., Läufer, A., Mayer, C., Tiedemann, R., Wilhelms, F., and Eisen, O.: Detailed Seismic Bathymetry Beneath Ekström Ice Shelf, Antarctica: Implications for Glacial History and Ice-Ocean Interaction, Geophysical Research Letters, 47, https://doi.org/10.1029/2019GL086187, 2020a.

Smith, E. C., Hattermann, T., Kuhn, G., Gaedicke, C., Berger, S., Gromig, R., Haas, C., Läufer, A. L., Tell, J., Tiedemann, R., Tison, J.-L., Wilhelms, F., and Eisen, O.: CTD profiles from beneath Ekstroem Ice Shelf and Atka Bay, https://doi.org/10.1594/PANGAEA.914478, 2020b.

Sweeney, C., Gloor, E., Jacobson, A. R., Key, R. M., McKinley, G., Sarmiento, J. L., and Wanninkhof, R.: Constraining global air-sea gas exchange for CO_2 with recent bomb 14C measurements, Global Biogeochemical Cycles, 21, 1–10, https://doi.org/10.1029/2006GB002784, 2007.

Thompson, A. F., Stewart, A. L., Spence, P., and Heywood, K. J.: The Antarctic Slope Current in a Changing Climate, Reviews of Geophysics, 56, 741–770, https://doi.org/10.1029/2018RG000624, 2018.

Wanninkhof, R.: Relationship between wind speed and gas exchange over the ocean, Journal of Geophysical Research, 97, 7373–7382, https://doi.org/10.1029/92JC00188, 1992.

Wanninkhof, R.: Relationship between wind speed and gas exchange over the ocean revisited, Limnology and Oceanography: Methods, 12, 351–362, https://doi.org/10.4319/lom.2014.12.351, 2014.

Weiss, R. F.: Carbon dioxide in water and seawater: The solubility of a non-ideal gas, Marine Chemistry, 2, 203–215, 1974.

Weiss, R. F. and Price, B. A.: Nitrous oxide solubility in water and seawater, Marine Chemistry, 8, 347–359, 1980.

https://doi.org/10.5194/os-2022-19
Preprint. Discussion started: 1 April 2022

Witte, H. and Boebel, O.: Processed 2 minutes-averaged continuous VM-ADCP (vessel-mounted Acoustic Doppler Current Profiler) profiles during POLARSTERN cruise PS89, https://doi.org/10.1594/PANGAEA.885934, 2018.

Zhou, Q., Hattermann, T., Nost, O., Biuw, M., Kovacs, K. M., and Lydersen, C.: Wind-driven spreading of fresh surface water beneath ice shelves in the eastern Weddell Sea, Journal of Geophysical Research: Oceans, 119, 3818–3833, https://doi.org/10.1002/2013JC009556.Received, 2014.